PLOS GENETICS

RESEARCH ARTICLE

Mitochondrial proline catabolism activates Ras1/cAMP/PKA-induced filamentation in *Candida albicans*

Fitz Gerald S. Silao, Meliza Ward, Kicki Ryman, Axel Wallström, Björn Brindefalk, Klas Udekwu, Per O. Ljungdahl*

Department of Molecular Biosciences, The Wenner-Gren Institute, Stockholm University, Stockholm, Sweden

* per.ljungdahl@su.se

OPEN ACCESS

Citation: Silao FGS, Ward M, Ryman K, Wallström A, Brindefalk B, Udekwu K, et al. (2019) Mitochondrial proline catabolism activates Ras1/cAMP/PKA-induced filamentation in *Candida albicans*. PLoS Genet 15(2): e1007976. https://doi.org/10.1371/journal.pgen.1007976

Editor: Aaron P. Mitchell, Carnegie Mellon University, UNITED STATES

Received: January 7, 2019

Accepted: January 21, 2019

Published: February 11, 2019

Data Availability Statement: All relevant data are within the manuscript and its Supporting Information files.

Funding: This work was supported by EU grant MC-ITN-606786 (ImResFun) and Swedish Research Council VR-2015-04202 (POL). The funders had no role in study design, data collection and analysis, decision to publish, or preparation of the manuscript.

Competing interests: The authors have declared that no competing interests exist.

Abstract

Amino acids are among the earliest identified inducers of yeast-to-hyphal transitions in *Candida albicans*, an opportunistic fungal pathogen of humans. Here, we show that the morphogenic amino acids arginine, ornithine and proline are internalized and metabolized in mitochondria via a *PUT1*- and *PUT2*-dependent pathway that results in enhanced ATP production. Elevated ATP levels correlate with Ras1/cAMP/PKA pathway activation and Efg1-induced gene expression. The magnitude of amino acid-induced filamentation is linked to glucose availability; high levels of glucose repress mitochondrial function thereby dampening filamentation. Furthermore, arginine-induced morphogenesis occurs more rapidly and independently of Dur1,2-catalyzed urea degradation, indicating that mitochondrial-generated ATP, not CO_2, is the primary morphogenic signal derived from arginine metabolism. The important role of the SPS-sensor of extracellular amino acids in morphogenesis is the consequence of induced amino acid permease gene expression, i.e., SPS-sensor activation enhances the capacity of cells to take up morphogenic amino acids, a requisite for their catabolism. *C. albicans* cells engulfed by murine macrophages filament, resulting in macrophage lysis. Phagocytosed *put1-/-* and *put2-/-* cells do not filament and exhibit reduced viability, consistent with a critical role of mitochondrial proline metabolism in virulence.

Author summary

Candida albicans is an opportunistic fungal pathogen that exists as a benign member of the human microbiome. Immunosuppression, or microbial dysbiosis, can predispose an individual to infection, enabling this fungus to evade innate immune cells and initiate a spectrum of pathologies, including superficial mucocutaneous or even life-threatening invasive infections. Infectious growth is attributed to an array of virulence characteristics, a major one being the ability to switch morphologies from round yeast-like to elongated hyphal cells. Here we report that mitochondrial proline catabolism is required to induce hyphal growth of *C. albicans* cells in phagosomes of engulfing macrophages, which is key to evade killing by macrophages. The finding that proline catabolism, also required for the utilization of arginine and ornithine, is required to sustain the energy demands of hyphal

growth underscores the central role of mitochondria in fungal virulence. In contrast to existing dogma, we show that in *C. albicans*, mitochondrial function is subject to glucose repression, amino acid-induced signals are strictly dependent on Ras1 and the SPS-sensor is the primary sensor of extracellular amino acids. The results provide a clear example of how *C. albicans* cells sense and respond to host nutrients to ensure proper nutrient uptake and survival.

Introduction

Candida albicans is an opportunistic fungal pathogen that commonly exists as a benign member of the human microbiome. Immunosuppression, or microbial dysbiosis, can predispose an individual to infection, enabling this fungus to initiate and develop a spectrum of pathologies, including superficial mucocutaneous or even life-threatening invasive infections [1, 2]. As a human commensal, *C. albicans* can asymptomatically colonize virtually all anatomical sites in the host, each with a characteristic and unique microenvironment, with differing nutrient and microbiome compositions, physical properties, and levels of innate immune defenses [3]. The ability to colonize and infect discrete microenvironments is attributed to an array of virulence characteristics, a major one being its morphological plasticity. As a pleomorphic organism, *C. albicans* can assume at least three distinct morphologies: yeast-like, pseudohyphae, and true hyphae, where the latter two are commonly referred to as filamentous morphologies (for review see [4–7]). Strains that are genetically locked in either yeast or filamentous forms fail to mount infections *in vitro* and *in vivo* infection models, supporting the concept that morphological switching, rather than the specific morphology *per se*, is a requisite to virulence [4, 6, 8–10]. The environmental signals known to trigger morphogenesis in *C. albicans* reflect the conditions within the human host, such as temperature (37 ˚C), CO_2, alkaline pH, the presence of serum, N-acetylglucosamine, and a discrete set of amino acids.

Early studies examining amino acid-induced morphogenesis implicated metabolism as being important for filamentation, and the inducing effects were shown to correlate to the specific point-of-entry in metabolism [11–13]. The most potent inducers of filamentation are amino acids that are catabolized to glutamate, such as arginine and proline, which enters the TCA cycle via α-ketoglutarate. Importantly, arginine and proline can supply nitrogen and carbon for intermediary metabolism and their catabolism provides energy to support diverse cellular functions. Studies examining proline uptake and distribution during filamentous growth suggested that proline catabolism results in an increase in the cellular reducing potential, i.e., enhanced levels of reduced flavoproteins were noted [11]. Several of the conclusions from these earlier studies, in particular that filamentous growth of *C. albicans* is linked to repression of mitochondrial activity [11–13], appear to conflict with more recent reports showing that filamentation is dependent on mitochondrial respiratory activity [14–18]. Clearly, the underlying mechanisms through which amino acids induce filamentation remain to be defined. In particular, the basis of arginine- and proline-induced morphogenesis needs to be placed in context to the current mechanistic understanding of the signaling cascades implicated in morphogenesis.

Among the central metabolic signaling pathways in *C. albicans* linked to morphogenesis, the best characterized are the mitogen-activated protein kinase (MAPK) and the 3'-5'-cyclic adenosine monophosphate/Protein Kinase A (cAMP/PKA) signaling systems, which activate the transcription factors Cph1 and Efg1, respectively [8, 19, 20], reviewed in [4, 7, 21, 22]. Ras1 is a small GTPase required for proper MAPK and cAMP/PKA signaling, and specifically for

the induction of filamentation by amino acids and serum [23, 24], reviewed in [22, 25]. Recently, Grahl et al. have proposed that intracellular ATP levels and increased mitochondrial activity control the activation of Ras1/cAMP/PKA pathway [14]. In this intriguing model, the adenyl cyclase (Cyr1/Cdc35) works cooperatively in a positive feedback loop with ATP as key input. Accordingly, ATP promotes Cyr1 binding to the active GTP-bound form of Ras1 thereby reducing the ability of Ira2 to stimulate the intrinsic GTPase activity of Ras1. As a consequence, enhanced Cyr1 activity leads to elevated levels of cAMP and amplification of PKA-dependent signaling, activating the effector transcription factor Efg1 and the expression of genes required for filamentous growth [26–28], reviewed in [22, 25, 29, 30].

Some morphogenic signals appear to bypass the requirement for Ras1 (reviewed in [29, 30]). By example, CO_2 is a well-characterized stimulus for morphological switching in *C. albicans*; CO_2 binds directly and activates Cyr1 [31]. Ghosh et al. have proposed that arginine-induced morphogenesis is the consequence of arginase (*CAR1)* dependent metabolism to ornithine and urea, and subsequent urea amidolyase (*DUR1,2*)-dependent generation of CO_2 from urea [32]. Also, the G protein-coupled receptor Gpr1, which has been implicated in amino acid-induced morphogenesis, does not appear to require Ras1. Gpr1-initiated signals activate Cyr1 by stimulating GTP-GDP exchange on the Gα protein Gpa2; the active GTP-bound form of Gpa2 is thought to bind to the Gα-binding domain within the N-terminal of Cyr1 leading to enhanced cAMP production (reviewed in [22, 30]). It has been reported that Gpr1 senses the presence of extracellular methionine [33] and glucose [34], however recently, lactate has been proposed to be the primary activating ligand [35]. The role of Gpr1 in amino acid-induced morphogenesis remains an open question.

C. albicans cells respond to the presence of extracellular amino acids using the plasma membrane-localized SPS (Ssy1-Ptr3-Ssy5) sensor complex [36–38]. In response to amino acids, the primary sensor Ssy1 (Csy1) is stabilized in a signaling conformation leading to Ssy5-mediated proteolytic processing of two latently expressed transcription factors, Stp1 and Stp2 [36]. The processed factors efficiently target to the nucleus activating the expression of distinct sets of genes required for assimilation of external nitrogen. Stp1 regulates the expression of *SAP2*, encoding the major secreted aspartyl proteinase, and oligopeptide transporters (*OPT1* and *OPT3*); whereas Stp2 derepresses the expression of a subset of amino acid permeases (AAP) that facilitate amino acid uptake. *STP1* expression is controlled by nitrogen catabolite repression (NCR), a supra-regulatory system that represses that utilization of non-preferred nitrogen sources when preferred ones are available [39]. The endoplasmic reticulum (ER)-localized chaperone Csh3 is required for the functional expression of both Ssy1 and AAPs, and thus acts as the most upstream and downstream component of the SPS sensing pathway [37]. Strains lacking either Ssy1 or Csh3 fail to efficiently respond to the presence of extracellular amino acids and serum and exhibit impaired morphological switching [37, 38]. It has not previously been determined if the SPS-sensor induces morphogenesis directly in response to extracellular amino acids, or indirectly, the consequence of enhanced amino acid uptake and subsequent intracellular signaling events.

In this report, we show how amino acid-induced and SPS-sensor-dependent signals are integrated into the central signaling pathways that control yeast-to-hyphal morphological transitions in *C. albicans*. Our results indicate that the augmented levels of intracellular ATP, resulting from catabolism of proline in the mitochondria, correlate with activated Ras1/cAMP/PKA and Efg1-dependent gene expression. The magnitude of the response is sensitive to the levels of glucose in a manner consistent with glucose repression of mitochondrial function. The SPS-sensor plays an indirect, but important, role in enhancing the uptake of the inducing amino acids. Finally, we show that *C. albicans* cells express proline catabolic enzymes when phagocytosed by murine macrophages, and that inactivation of proline

catabolism diminishes the capacity of *C. albicans* cells to induce hyphal growth and escape engulfing macrophages.

Results

Amino acid-induced morphogenesis is dependent on uptake

We assessed the capacity of ornithine, citrulline, and the 20 amino acids commonly found in proteins to induce filamentous growth in *C. albicans*. Wildtype (WT) cells were grown as macrocolonies on MES-buffered (pH of 6.0) synthetic dextrose (2% glucose) medium containing 10 mM of each individual amino acid as sole nitrogen source. As shown in Fig 1A, proline and arginine strongly induced filamentous growth as evidenced by the formation of wrinkled macrocolonies. Microscopic evaluation of cells from wrinkled colonies confirmed filamentous growth (mainly hyphal). Ornithine, a non-proteinogenic amino acid and a catabolic intermediate in the degradation of arginine, induced pronounced filamentous growth. Of the amino acids tested, aspartate consistently produced smooth macrocolonies comprised of round cells exclusively yeast-like in appearance. Consequently, aspartate was chosen as a negative reference control for subsequent studies.

Using quantitative RT-PCR (qRT-PCR), we analyzed the expression of known hyphae-specific genes (HSG) *ECE1*, *EED1*, *HWP1*, *UME6*, *ALS3*, *HGC1*, *SAP4*, and *SAP5* [4] in cells from colonies grown on media with arginine, proline, ornithine and aspartate. With the exception of *EED1*, the expression of HSG were clearly induced in cells grown on media with morphogenic amino acids, $\geq$ 7-fold higher than in cells grown on aspartate (S1 Fig). *SAP4*, a known Efg1-regulated gene [40], exhibited the highest level of induction, $\geq$ 80-fold higher levels than in aspartate grown cells. These experiments were repeated using liquid cultures, and the same trends were observed. These results confirm the appropriateness of using macrocolonies to score amino acid-induced morphogenesis.

Next, we evaluated whether SPS-sensor activation was required for amino acid-induced morphogenesis. This was accomplished by assessing SPS-sensor dependent Stp2 processing [36]. A strain carrying a functional C-terminal HA tagged Stp2 (Stp2-HA; PMRCA44) was grown in minimal ammonium-based synthetic dextrose (SD) medium, extracts were prepared 5 min after induction by the indicated amino acid. Arginine (R), asparagine (N), aspartate (D), glutamine (Q), histidine (H), lysine (K), serine (S) and ornithine (Orn) efficiently activated the SPS-sensor; extracts contained the shorter processed form of Stp2 (Fig 1B, upper panel). Next, we assessed Stp2-dependent promoter activation using an integrated P_{CAN1}-NanoLuc-PEST reporter construct; the expression of the luciferase signal is controlled by the *CAN1* promoter, which is strictly dependent on the SPS-sensor and Stp2 (S2 Fig). The inclusion of the 41-amino acid PEST sequence confers a shorter NanoLuc lifetime, which facilitates a tighter coupling of transcription and translation [41]. Enhanced luminescence was observed only in cells induced with the amino acids giving rise to Stp2 processing (Fig 1B, lower panel). Notably, proline, which induces robust filamentation, did not activate the SPS-sensor as no Stp2 processing or luminescence was detected. Conversely, aspartate, which does not induce filamentous growth, robustly activated the SPS-sensor as determined by Stp2 processing and enhanced luciferase activity. These results indicate that amino acid-induced morphogenesis is not obligatorily coupled to SPS-sensor signaling.

The contribution of signals derived from the SPS sensing pathway on filamentation induced by arginine, ornithine and proline was examined. Arginine, a potent inducer of the SPS-sensor (Fig 1B), induced filamentation in an SPS-sensor independent manner; filamentation was observed in mutants lacking components of the SPS sensing pathway (Fig 1C). By contrast, ornithine, also a potent inducer of the SPS-sensor, induced filamentous growth in a strictly

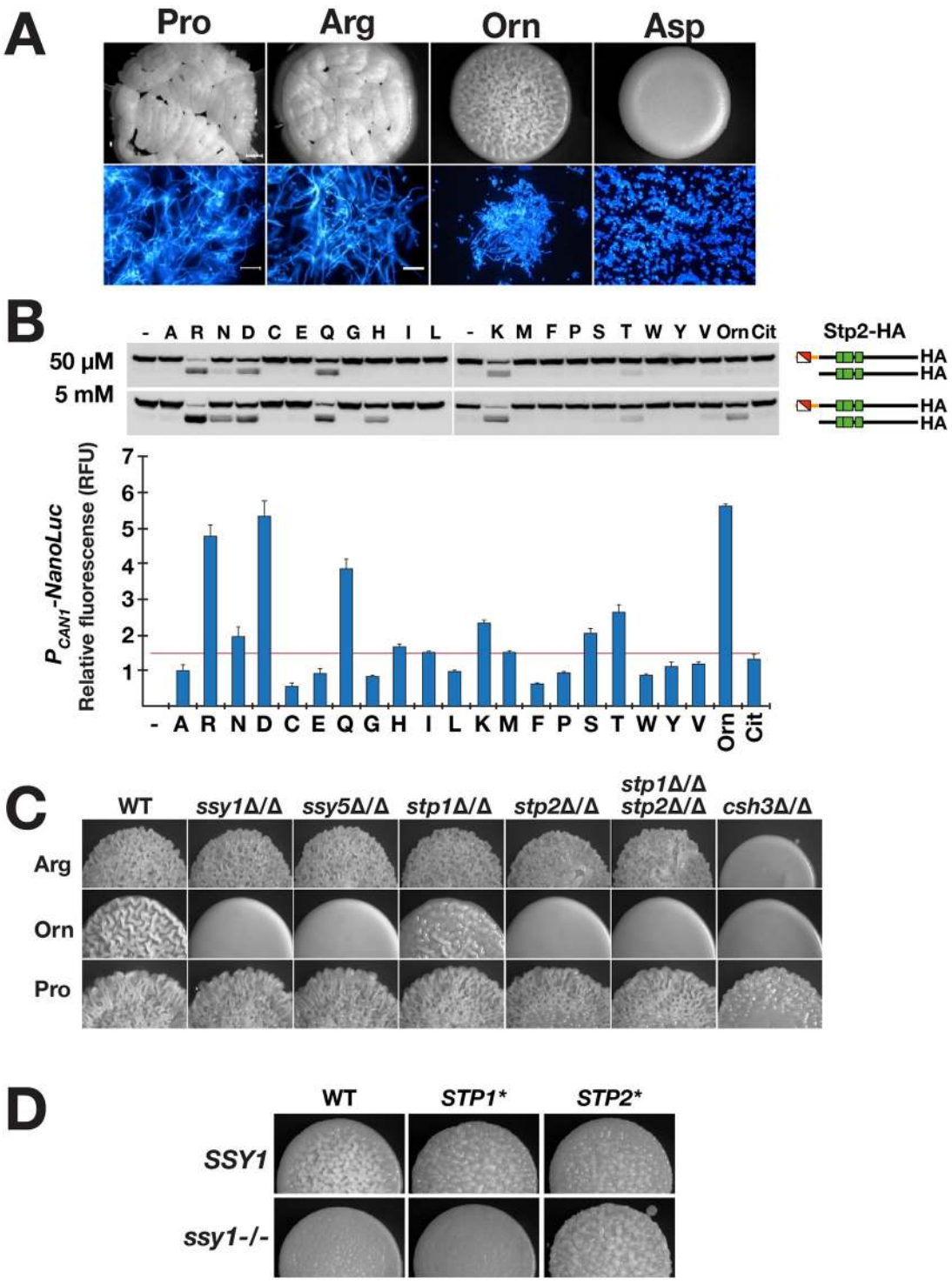

Fig 1. Amino acid-induced morphogenesis is dependent on amino acid uptake. A. Macrocolonies of wildtype *C. albicans* (PMRCA18) grown on SXD medium containing 10 mM of the indicated amino acids (X = Pro, Arg, Orn or Asp) and 2% glucose after 48 h of growth at 37 ˚C (upper panels). Cells scraped from macrocolonies stained with calcofluor white (lower panels); scale bars = 30 μ. **B**. Amino acid-induced SPS-sensor signaling. Cells expressing Stp2-6XHA (PMRCA48) were grown to log phase in SD medium and induced with 50 μM or 5 mM of the indicated amino acids for 5 min at 30 ˚C. The levels of latent and processed Stp2 in extracts were analyzed by immunoblotting (upper panels). Similarly, reporter strain (CFG001) carrying an integrated P_{CAN1}-NanoLuc-PEST construct was grown to log phase in SD medium and induced with 50 μM of the indicated amino acids for 2 h at 30 ˚C. The average luciferase signal (ave. ± CI, 95% CL) are plotted; threshold for significance ≥ 1.5X fold change). **C**.

Macrocolonies of wildtype (WT; PMRCA18) and strains carrying mutations inactivating SPS-sensing pathway components *ssy1*Δ/Δ (YJA64), *ssy5*Δ/Δ (YJA53), *stp1*Δ/Δ (PMRCA59), *stp2*Δ/Δ (PMRCA57), *stp1*Δ/Δ *stp2*Δ/Δ (PMRCA94) and *csh3*Δ/Δ (PMRCA12) grown on the indicated SXD media. **D**. Constitutively active Stp2* but not Stp1* bypasses the filamentous growth defect of a *ssy1* null mutant in the presence of ornithine. Macrocolonies of WT (PMRCA18), *STP1** (PMRCA23), *STP2** (PMRCA44), *ssy1*-/- *STP1** (CFG078), and *ssy1*-/- *STP2** (CFG073) grown on SOD with ornithine (O) as sole nitrogen source. Images in **C** and **D** were obtained after 24 h of incubation 37 ˚C.

https://doi.org/10.1371/journal.pgen.1007976.g001

SPS-sensor- and Stp2-dependent manner (Fig 1C). Notably, Stp1, a transcription factor that induces genes required for extracellular protein utilization, is not required for ornithine-induced filamentation. Proline, which does not induce SPS-sensor signaling, promoted filamentous growth in an SPS-sensor independent manner (Fig 1C). Importantly, the filamentation was greatly reduced in cells lacking *CSH3* (*csh3*Δ/Δ), encoding a membrane-localized chaperone required for the functional expression of Ssy1 and most amino acid permeases [37, 38] (Fig 1C and S3B Fig), suggesting that amino acid uptake is required for amino acid-induced morphogenesis.

The clear requirement of the SPS-sensor in facilitating ornithine-induced filamentation provided the opportunity to rigorously test the notion that uptake is essential. Based on the knowledge that amino acid permease-dependent uptake is dependent on Stp2 and not Stp1, we used the CRISPR/Cas9 system to introduce *ssy1* null mutations in strains expressing constitutively active Stp2 (*STP2**) or Stp1 (*STP1**) [36] (S3A Fig). The results clearly show that *STP2**, but not *STP1** (Fig 1D), bypasses the *ssy1* null mutation, indicating that the permeases responsible for ornithine uptake are encoded by a SPS-sensor and Stp2 controlled genes. Similarly, SPS-sensor dependence was observed for the inducing amino acids alanine, glutamine, and serine. Together, these results indicate that amino acid-induced filamentous growth is dependent on the uptake of the inducing amino acid.

Amino acid-induced morphogenesis is dependent on catabolism and Ras1/cAMP/PKA signaling

Two core signaling pathways, i.e., MAPK and cAMP/PKA, are known to transduce metabolic signals that affect filamentous growth (Fig 2A). We evaluated the capacity of amino acids to induce filamentation in cells carrying null alleles of *RAS1* and the effector transcription factors, *CPH1* and *EFG1* diagnostic for MAPK and cAMP/PKA signaling, respectively [8, 20, 42](Fig 2B). Similar to wildtype, *cph1*Δ/Δ cells were wrinkled in appearance, indicating that amino acid induced filamentation was largely independent of MAPK signaling. By contrast, the colonies derived from *ras1*Δ/Δ and *efg1*Δ/Δ cells were smooth. As expected, the *efg1*Δ/Δ *cph1*Δ/Δ double mutant strain also formed smooth colonies. These results indicate that the inducing signals are primarily transduced by the cAMP/PKA pathway. A clear dependence on Ras1/cAMP/PKA signaling was also observed for other inducing amino acids, i.e., alanine, glutamine, and serine (S7A Fig). Our results demonstrating that amino acid-induced morphogenesis is strictly dependent on Ras1 is contrary to current models that postulate that amino acids-initiated signals are transduced by Gpr1/Gpa2 (reviewed in [22, 30]). According to these models, amino acid signaling should be Ras1 independent.

The finding that amino acid-induced morphogenesis is Ras1 dependent suggested that amino acid-initiated signals promote GTP-GDP exchange. To test this notion, we assessed the levels of Ras1-GTP in cells after induction by amino acids (Fig 2C). Our results clearly show that in contrast to cells induced with aspartate, cells induced with arginine, proline and ornithine possess increased levels of activated Ras1 in its GTP bound form. Consistent with this observation, inactivation of *IRA2* led to constitutive hyphal growth in YPD at 30 ˚C,

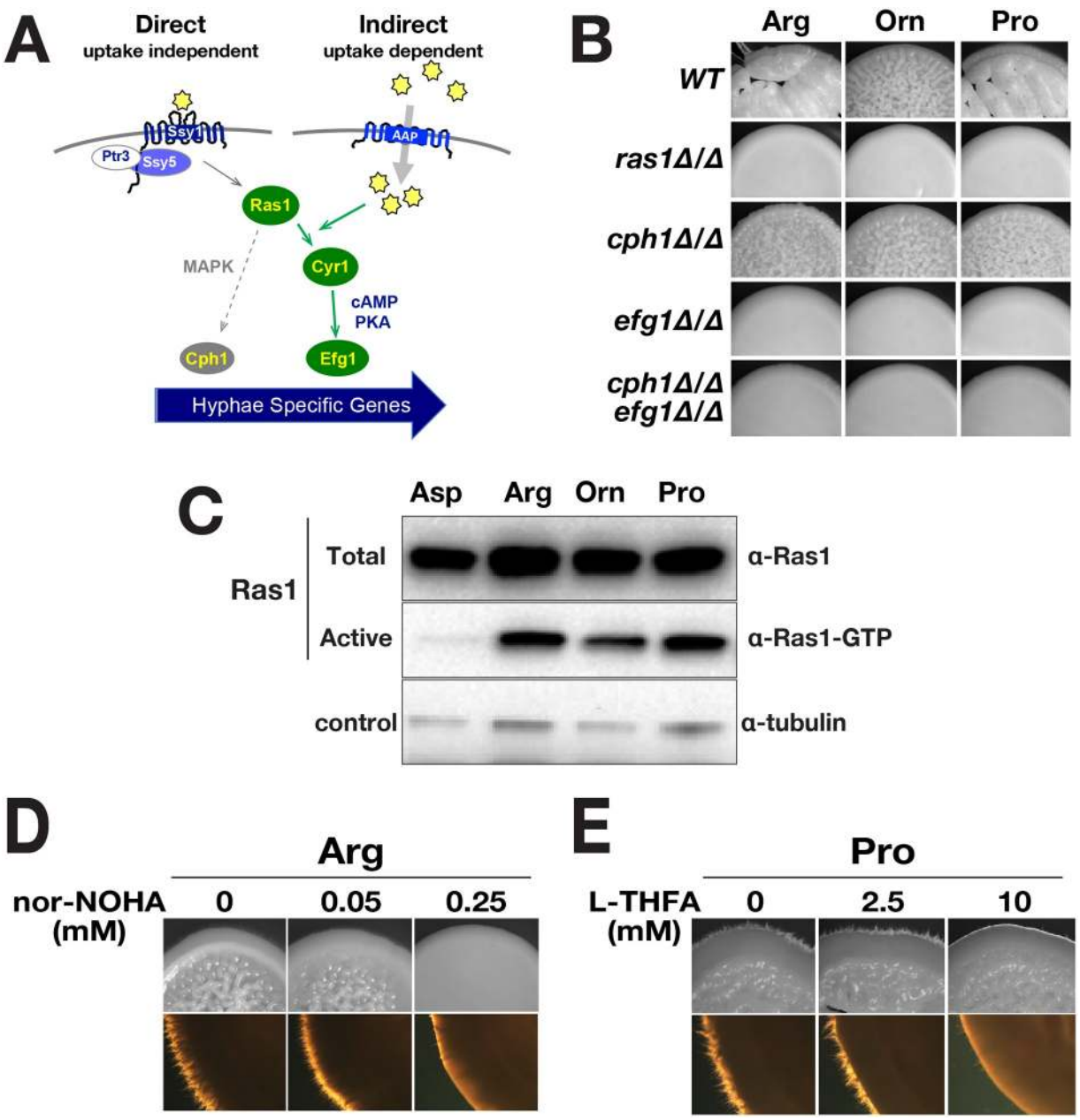

Fig 2. Amino acid-induced morphogenesis is dependent on catabolism and Ras1 activated Efg1-dependent transcription. A. Scheme of possible signaling pathways controlling amino acid-induced morphogenesis. **B**. Amino acid-induced morphogenesis requires a functional Ras1/cAMP/PKA pathway (Efg1-dependent) but not on the MAPK signaling pathway (Cph1-dependent). Wildtype (WT; PMRCA18) and strains lacking Ras1 (CDH107), Cph1 (JKC19), Efg1 (HLC52), and both Cph1 and Efg1 (HLC54) were spotted onto the indicated SXD media (X = Pro, Arg, Orn or Asp) and incubated at 37 ˚C for 48 h. **C**. Levels of active GTP bound form of Ras1 (Ras1-GTP) increase upon amino acid induction. Extracts were prepared from pooled WT (PMRCA18) macrocolonies grown for 24 h at 37 ˚C on the specified SXD medium. The levels of total Ras1 and the activated forms (Ras1-GTP) were determined by immunoprecipitation. **D**. Arginine catabolism is required for arginine-induced morphogenesis. Cells were spotted on SRD (Arg) supplemented with nor-NOHA, a competitive inhibitor of arginase. **E**. Proline catabolism is required for proline-induced morphogenesis. Cells were spotted on SPD (Pro) supplemented with L-THFA, a competitive inhibitor of proline dehydrogenase. For **D** and **E**, macrocolonies (PMRCA18) were grown at 37 ˚C and photographed after 72 h. Lower images are magnified 2X in comparison to upper images.

https://doi.org/10.1371/journal.pgen.1007976.g002

conditions that normally do not induce hyphal growth (S3C Fig). In an attempt to directly assess the requirement of adenylyl cyclase we obtained the characterized *cdc35*Δ/Δ (*cyr1*) strain [28]. Contrary to expectations, this strain did not grow in the synthetic media used here, even when the media was supplemented with 100 μg/ml uridine and/or 10 mM dibutyryl cAMP. Unfortunately, the lack of growth precluded a direct assessment of the role of Cyr1.

We tested whether amino acid catabolism was required to activate PKA-signaling by examining the morphology of colonies from cells grown on medium containing arginine or proline as sole nitrogen source and enzyme specific inhibitors. In *C. albicans*, arginine is primarily catabolized via the arginase (*CAR1*) pathway to ornithine and urea. N^{ω}-hydroxy-nor-arginine (Nor-NOHA), a potent competitive inhibitor of arginase [43], inhibited arginine-induced filamentation in a dose-dependent manner (Fig 2D). Similarly, L-tetrahydrofuroic acid (L-THFA), a specific competitive inhibitor of proline dehydrogenase (Put1)[44, 45], greatly impaired filamentation in a dose-dependent manner (Fig 2E). The data demonstrate that the arginine- and proline-inducing signals are derived from their catabolism.

Increased ATP resulting from mitochondrial metabolism of morphogenic amino acids activate Ras1/cAMP/PKA signaling

Intracellular levels of ATP are thought to provide a key input for Ras1/cAMP/PKA signaling [14]. Consistent with this notion, in comparison to cells grown in the presence of non-inducing nitrogen sources, such as aspartate and ammonium sulfate, cells grown in the presence of the morphogenic amino acids arginine, ornithine or proline contained similar, and significantly higher levels of ATP (Fig 3A). Although urea is a good inducer of filamentous growth, urea grown cells contained low levels of ATP. This finding is consistent with previous reports that morphogenic induction by urea is dependent on *DUR1*,*2*-dependent metabolism that generates CO_2 [31, 32].

Arginine and ornithine are catabolized to proline in the cytoplasm, and proline is subsequently metabolized to glutamate and then α-ketoglutarate in the mitochondria [12]. These metabolic events generate the reduced electron donors, $FADH_2$ and NADH, which are oxidized by the mitochondrial electron transfer chain leading to ATP synthesis (Fig 3A). We posited that the increased levels of ATP resulting from the catabolism of arginine, ornithine and proline is the consequence of their shared metabolic pathway. To test this, we used methylene blue (MB), which effectively uncouples electron transport from the generation of a proton motive force generated by mitochondrial respiratory complexes I-III [46, 47]. The inclusion of MB in media containing ornithine or proline completely inhibited filamentous growth (Fig 3B). The inhibitory effect of MB in cells growing on arginine was not complete; a higher concentration of MB was required to noticeably inhibit filamentation, consistent with the generation of CO_2 by the *DUR1*,*2*-dependent metabolism of urea [32].

We sought independent means to assess levels of reduced electron donors generated by the metabolism of the morphogenic amino acids. The membrane-permeable redox indicator TTC (2,3,5 triphenyltetrazolium chloride, colorless) is converted to TTF (1,3,5-triphenylformazan, red) in the presence of NADH and has been be used to monitor mitochondrial respiratory activity of colonies [15, 48]. Colonies growing on proline, arginine, and ornithine exhibited a more intense, deep red pigment than colonies growing on aspartate (Fig 3C, top panel). The redox-sensitive dye resazurin can be used in liquid culture to monitor the reducing capacity of the intracellular environment [49]; resazurin is non-fluorescent, but is readily reduced by NADH or to a lesser extent by NADPH to highly red fluorescent resorufin (excitation 560 nm, emission 590 nm). Consistent with the results obtained using TTC, cells growing with proline, arginine, or ornithine as sole nitrogen source exhibited 6–8-fold more resorufin fluorescence

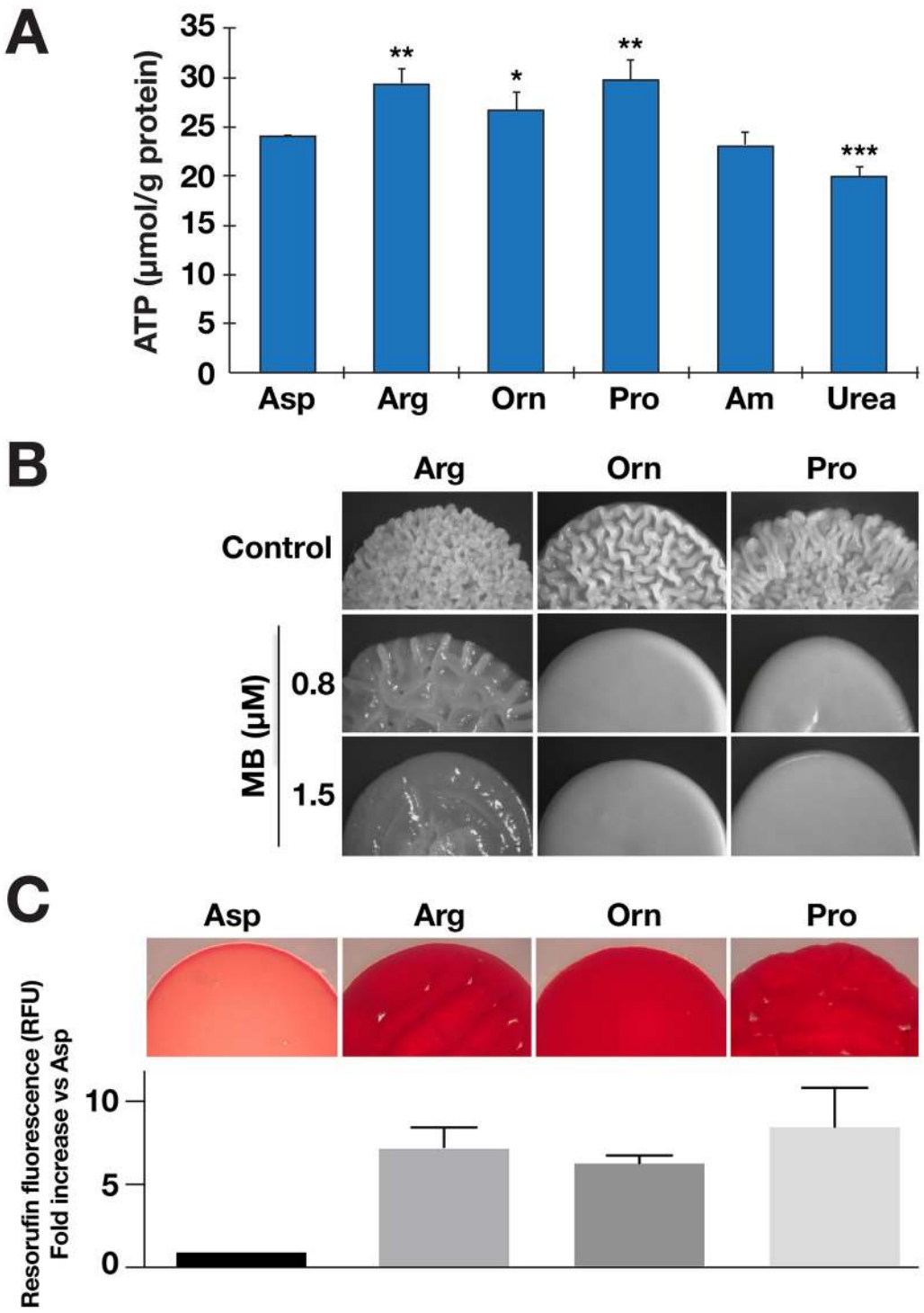

Fig 3. Amino acid-induced morphogenesis requires mitochondrial oxidative phosphorylation. A. ATP levels in macrocolonies (PMRCA18) formed 24 h after spotting cells on the indicated SXD medium (X = Asp, Arg, Orn, Pro, Am (ammonium sulfate) or Urea) incubated at 37 ˚C. The levels of ATP in three biological replicates normalized to total protein are plotted. The values from each biological replicate is the average of 2–3 technical replicates. Statistically significant changes in ATP levels, as compared to cells grown on Asp, are indicated (ave. ± CI; **, p value < 0.01; *, p value < 0.05). **B**. Uncoupling of mitochondria reduces amino acid-induced filamentation. Cells (PMRCA18) were spotted on SXD media (X = Arg, Orn or Pro) supplemented with indicated amount of methylene blue (MB); macrocolonies were grown at 37 ˚C and photographed after 24 h. **C**. Metabolic activity of *C. albicans* grown in the

presence of inducing and non-inducing amino acids. Mitochondrial respiratory activity of macrocolonies (PMRCA18) grown on the indicated solid media was assessed using the TTC-overlay method (upper panel; representative of three independent assessments) and the reduction of the nonfluorescent resazurin dye by NADH or NADPH oxidoreductases (lower panel). Fluorescence signals plotted were from the average of four biological replicates (ave. ± CI, 95% CL).

https://doi.org/10.1371/journal.pgen.1007976.g003

than aspartate grown cells (Fig 3C, bottom panel). These results indicate that cells grown in the presence of proline as the sole nitrogen source have a reducing intracellular environment, a finding aligned with the previous report by Land et al. [11].

Proline metabolism generates the primary signal for arginine-induced morphogenesis

Arginine is degraded in a pathway that bifurcates after the initial reaction catalyzed by Car1, which forms ornithine and urea (Fig 4A). Ornithine is subsequently metabolized by ornithine aminotransferase (*CAR2*) to form glutamate γ-semialdehyde, which spontaneously converts to Δ^1-pyrroline-5-carboxylate (P5C). P5C is converted to proline by the *PRO3* gene product. Cytoplasmic proline is transported into the mitochondria where it is converted back to P5C by proline oxidase (*PUT1*). Finally, the mitochondrial P5C is converted to glutamate by the *PUT2* gene product [50, 51], which is then converted to α-ketoglutarate via Gdh2. Urea is further catabolized in the cytosol by urea amidolyase (*DUR1,2*) forming NH_3 and CO_2.

Based on our results demonstrating that the filament-inducing effect of ornithine and proline requires mitochondrial respiration, we investigated if both branches of the bifurcated arginine degradative pathway could independently trigger filamentous growth. To accomplish this, we used a CRISPR/Cas9 strategy to construct PMRCA18-derived strains individually lacking *CAR1* (S3D Fig), *DUR1,2* (S3E Fig), or *PUT1*, *PUT2* and *PUT3* (S3F Fig), or both *PUT1* and *DUR1,2* (S3G Fig). Growth-based assays, on solid and in liquid media, confirmed that the *car1*-/- strain exhibited impaired growth on synthetic glucose medium (SXD) containing arginine as a sole nitrogen source, whereas the strain grew like wildtype (WT) on SXD medium containing either 10 mM ornithine, proline or urea (Fig 4B and S4 Fig). As expected, and similar to previous reports [32], the *dur1,2*-/- strain exhibited severely impaired growth on medium containing urea as sole nitrogen source, but grew well in media containing arginine, ornithine or proline as sole nitrogen sources (Fig 4B and S4 Fig). Cells lacking the proline oxidase (*put1*-/-) were able to grow in media containing arginine, but unable to grow when ornithine or proline were the sole source of nitrogen (Fig 4B and S4 Fig), indicating that ornithine utilization is strictly dependent on the mitochondrial proline catabolic pathway (Fig 4B and S4 Fig).

Quite surprisingly, in media with 2% glucose the *put1*-/- *dur1,2*-/- double mutant strain retained the ability to grow using arginine as sole nitrogen source, albeit slower, clearly suggesting that an arginase-independent pathway exists in *C. albicans* (Fig 4B and S4 Fig). Consistently, the *car1*-/- strain also exhibited residual growth using arginine as sole N-source in media with 2% glucose as primary carbon source. However, the *car1*-/- strain is unable to use arginine as the sole carbon source and did not grow in media lacking glucose (S3D and S5 Figs). Thus, the arginase-independent pathway enables the use of arginine merely as a nitrogen source.

Next, we analyzed the expression of genes involved in arginine catabolism in cells after shifting them to minimal medium containing 10 mM arginine (YNB+Arg) as sole nitrogen and carbon source (Fig 4C). One hour after the shift, the proline catabolic genes *PUT1* and *PUT2* were significantly upregulated. The levels of *PUT3*, the proline activated transcription factor that is constitutively bound to the promoter of *PUT1* and *PUT2*, did not change [52].

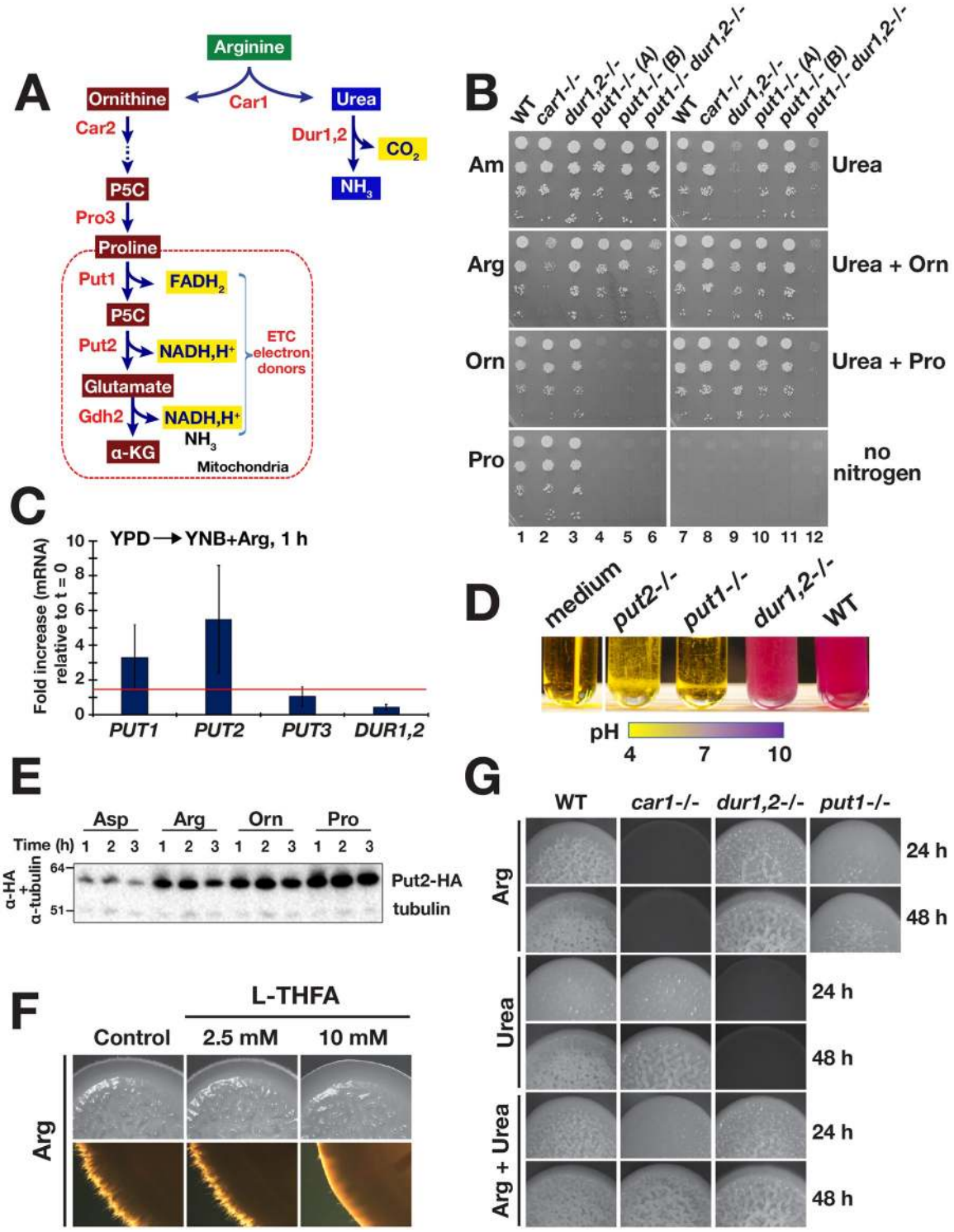

Fig 4. A bifurcated pathway for arginine-induced morphogenesis. A. Scheme of arginine catabolic pathway. **B**. Growth-based assays. Five microliters (5 μl) of serially diluted cells were spotted onto the surface of SXD (X = Am (Ammonium sulfate), Arg, Orn, Pro or Urea) and then grown for 48 h at 30˚C. Strains used: wildtype (WT; PMRCA18), *car1-/-* (CFG077), *dur1,2-/-* (CFG091), *put1-/-* (A) (CFG122), *put1-/-* (B) (CFG155), and *put1-/- dur1,2 -/-* (CFG158). **C**. Arginine rapidly derepresses proline catabolic genes. *PUT1*, *PUT2*, *PUT3* and *DUR1,2* expression in wildtype (SC5314) cells 1 h at 37 ˚C after shifting from YPD (t = 0) to YNB+Arg (pH = 6.0). Gene expression was determined by qRT-PCR using the levels of *RIP1* to normalize expression. **D**. Proline catabolic pathway is required for growth in arginine as a sole nitrogen and carbon source. Cells with the indicated genotypes were harvested from log phase YPD

cultures and diluted in YNB+Arg+BCP medium (pH = 4.0) to $OD_{600} \approx 0.01$, cultures were incubated for 16 h at 37 ˚C. Alkalization (shift to purple) correlates with growth. Strains used: WT (SC5314), *dur1,2*-/- (CFG246), *put1*-/- (CFG149), and *put2*-/- (CFG143). Identical results were obtained using PMRCA18-derived mutants. **E**. Rapid activation of proline catabolism in the presence of arginine, ornithine, and proline. Immunoblot analysis of Put2-HA in whole cell lysates prepared from CFG185 (*PUT2/PUT2-HA*) cells grown at 37 ˚C in the specified SXD media for the indicated times. Cells were pre-grown in YPD and inoculated at an OD_{600} of 0.5. Levels of α-tubulin were used as loading control. **F**. Pharmacological inhibition of proline dehydrogenase (Put1) reduced filamentous growth of *C. albicans* in the presence of arginine. Macrocolonies of wildtype (WT; PMRCA18) grown at 37 ˚C for 72 h on SRD medium supplemented with L-THFA as indicated. **G**. Filamentous growth of strains on SXD media (X = Arg, Urea, or Arg + Urea as sole nitrogen sources). Macrocolonies were grown at 37 ˚C and photographed at 24 and 48 h. Strains used: wildtype (WT; PMRCA18), *car1*-/- (CFG077), *dur1,2*-/- (CFG091), and *put1*-/- (CFG122).

https://doi.org/10.1371/journal.pgen.1007976.g004

Strikingly, *DUR1,2* gene expression remained constant. Contrary to the assumption that Dur1,2 is responsible for alkalization of the medium, the consequence of the deamination of arginine-derived urea [53], we observed that the *dur1,2*-/- mutant still alkalinized the medium (Fig 4D and S5 Fig). Notably, both *put1*-/- and *put2*-/- strains failed to grow in this medium (Fig 4D), indicating that the proline catabolic pathway branch of arginine utilization is essential for growth when arginine is both carbon and nitrogen source. Accordingly, an increased flux through the proline branch of the pathway and subsequent deamination of glutamate provides the likely explanation for the alkalization of the medium (Fig 4A).

Consistent with their ability to support growth, arginine, ornithine and proline induced the expression of HA epitope-tagged Put2 (Put2-HA) (Fig 4E). The induction was rapid, 1 h following the shift from YPD to SXD (X = 10 mM Asp, Arg, Orn or Pro); in the presence of arginine and ornithine, the Put2 levels were elevated and almost as high as in proline-induced cells. Aspartate did not induce Put2 expression. Together these results indicate that arginine and ornithine are efficiently metabolized to proline, and metabolism associated with proline branch is required for the use of these amino acids as energy sources for growth.

To test whether proline catabolism is required for arginine-induced morphogenesis, we tested whether filamentation would be reduced by inhibiting Put1 with L-THFA (Zhu et al., 2002; Zhang et al., 2015). As expected, L-THFA inhibited arginine-induced morphogenesis (Fig 4F). We then carried out a genetic analysis to dissect the pathway triggering filamentous growth in the presence of arginine. Consistent with the existing model for arginine-induced morphogenesis [32], the *car1*-/- strain formed extensively wrinkled colonies comprised mainly of filamentous cells in the presence of 10 mM urea (Fig 4G). However, in comparison to wildtype colonies growing on arginine media, wrinkling was delayed and was first noticeable after 48 h of incubation. On media with an equimolar amount of arginine and urea (Arg + Urea) the *car1*-/- strain developed wrinkled colonies clearly visible after only 24 h. These findings suggest that arginine metabolism via the proline branch induces filamentation more rapidly than the CO_2 (HCO_3^-) generated by the Dur1,2-dependent degradation of urea. Consistent with this notion, colonies formed by the *put1*-/- mutant remained relatively smooth even after 48 h of growth (Fig 4G). In summary, our results indicate that the metabolism associated with proline branch of the arginine degradation pathway generates the primary and most rapid signal of arginine-induced morphogenesis.

Proline utilization is sensitive to carbon source availability and independent of NCR control

The capacity of proline to stimulate filamentous growth is significantly affected by glucose availability (Fig 5A). In comparison to colonies formed on synthetic media with 10 mM proline containing 2% glucose (SPD), colonies on media containing 0.2% glucose ($SPD_{0.2\%}$) exhibited larger feathery zones of hyphal cells emanating around their periphery. These

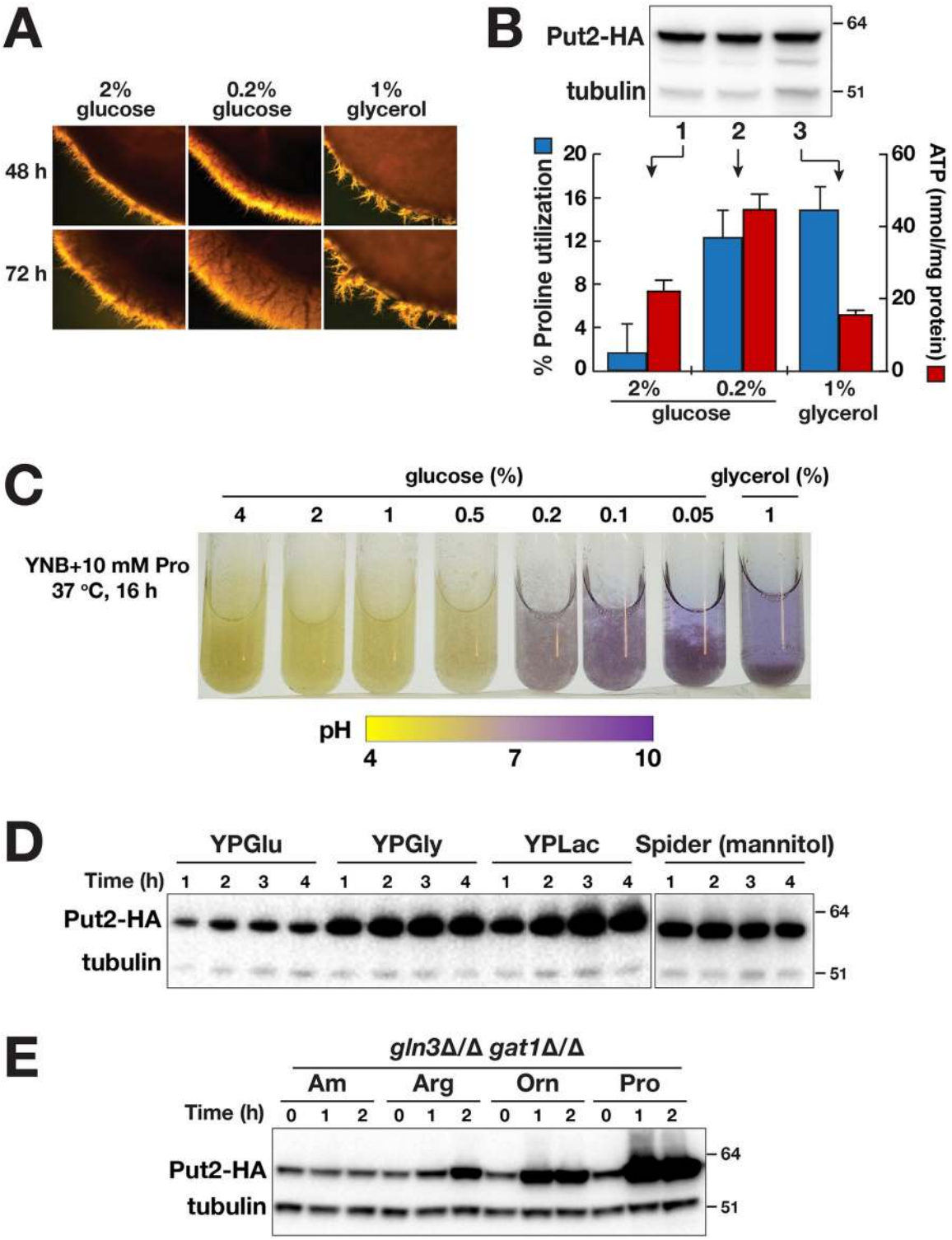

Fig 5. Proline utilization is influenced by carbon source but not by NCR. A. Filamentous growth is more robust at lower glucose level. Wildtype cells (PMRCA18) from overnight YPD liquid cultures were washed and then adjusted to OD_{600} of 8, 10 μl aliquots were spotted on media containing 10 mM of proline and the indicated levels of carbon source. Plates were incubated at 37 ˚C and photographed at 48 and 72 h. **B**. The rate of proline utilization and ATP levels are higher under glucose limited conditions. The levels of proline remaining in culture supernatants (blue bars, left axis) and ATP (red bars, right axis) of WT (PMRCA18) after 2 h of growth at 37 ˚C in the presence of different carbon source are indicated. Results shown are from 5 biological replicates (Ave. ± CI, 95% CL, p value < 0.001). Immunoblot analysis of Put2-HA and α-tubulin (loading control) in cell extracts prepared from CFG185 (*PUT2*/

PUT2-HA) grown under identical conditions (inset). **C**. Respiratory growth predominates as glucose level decreases. WT cells were diluted to OD_{600} of 0.5 in pre-warmed synthetic proline media containing 10 mM proline (YNB+Pro+BCP) and the indicated levels of glucose with the initial pH adjusted to 6.0. Cultures were grown for 16 h under vigorous agitation at 37 ˚C prior to photographing the culture tubes. Glycerol was used as respiratory growth control. **D**. Put2 is highly expressed in cells grown in the presence of non-glucose carbon sources. Immunoblot analysis of cell extracts prepared from CFG185 (*PUT2/PUT2-HA*) cells grown in YPGlu (YP+2% glucose = YPD), YPGly (YP + 1% glycerol), YPLac (YP + 1% lactate), or Spider medium (with 1% mannitol) at 37 ˚C for the timepoints indicated. Cells were pre-grown in YPD and inoculated at an OD_{600} of 0.5. **E**. Proline utilization is insensitive to NCR. Immunoblot analysis of cell extracts prepared from CFG184 (*gln3*Δ/Δ *gat1*Δ/Δ *PUT2/PUT2-HA*) grown at 30 ˚C in $SD_{0.2\%}$ medium, which contains 10 mM ammonium sulfate (Am) and 0.2% glucose, supplemented with 10 mM of the nitrogen sources and harvested at the timepoints as indicated. Cells were pre-grown in SD and cultured to log phase in $SD_{0.2\%}$.

https://doi.org/10.1371/journal.pgen.1007976.g005

findings are reminiscent of reports that *C. albicans* cells grown on media with methionine as nitrogen source and low glucose exhibit robust filamentation [33].

Next, we considered the possibility that glucose repression of mitochondrial function, known to occur in *Saccharomyces cerevisiae* [54, 55], may underlie the difference. At low glucose concentrations, i.e., non-repressing conditions, we expected that cells would use proline as an energy source to generate ATP. Proline utilization was assayed directly by measuring the amount of residual proline in culture supernatants after a 2 h incubation period. In media containing 2% glucose, cells took up $< 2\%$ of the proline. By contrast, cells growing in low glucose (0.2%) or 1% glycerol used 12–15% of the available proline (Fig 5B, blue bars). The levels of Put2 were similar indicating that its expression is independent of glucose (Fig 5B, insert). These results indicate that proline is taken up and metabolized more efficiently in cells under non-repressing conditions. Consistently, cells grown in the presence of 0.2% glucose had the highest levels of ATP, roughly 2-fold more ATP than cells grown in either 2% glucose or 1% glycerol (Fig 5B, red bars). These results are consistent with mitochondrial activity in *C. albicans* being subject to glucose repression.

To critically test this, we assessed the effect of varying the glucose concentration from 0.05–4%. Cells were grown for 16 h in media containing the pH indicator bromcresol purple. At high glucose concentrations (0.5–4%) the media remained acidic, indicating cells were growing fermentatively using proline merely as a nitrogen source (Fig 5C). By contrast, at glucose concentrations $\leq 0.2\%$, the media became alkaline, indicating that cells were respiring and using proline as the primary energy source. The increased flux through the proline pathway is expected to yield elevated NH_3 generated by the mitochondrial glutamate dehydrogenase (*GDH2*) catalyzed deamination of glutamate. To directly assess mitochondrial activity under these conditions, we carried out extracellular oxygen consumption analysis in a high-throughput microplate format (S6A and S6B Fig). Cells grown in repressing $SPD_{2\%}$ exhibited the lowest oxygen consumption whereas those grown at $SPD_{0.2\%}$ had the highest consumption, higher than cells grown in SPG. As previously pointed out, Put2 levels were similar across all conditions (Fig 5B). Together, these results indicate that proline is taken up and then metabolized more efficiently in cells growing under low glucose concentrations. Consistently, Put2 levels were elevated in rich media containing yeast extract and peptone when non-repressing, non-fermentative carbon sources replaced glucose; i.e., glycerol or lactate (Fig 5D). Similarly, cells express elevated levels of Put2 when grown in hyphal inducing Spider medium, a medium rich in amino acids and mannitol as a primary carbon source.

Nitrogen regulation of transcription in fungi is a supra-pathway response that is commonly referred to as nitrogen catabolite repression (NCR), which functions to ensure that cells selectively use preferred nitrogen sources when available. Briefly, NCR regulates the activity of GATA transcription factors Gln3 and Gat1; in the presence of preferred nitrogen sources, these factors do not gain access to the promoters of NCR-regulated genes (reviewed in [56]). Previous studies have shown that certain amino acids, traditionally classified as poor (e.g.,

proline) in *S. cerevisiae*, were readily utilized by *C. albicans* mutants lacking Gln3 and Gat1 [57]; the introduction of null alleles of both *GLN3* and *GAT1* in *C. albicans* did not impair growth using proline as sole nitrogen source, whereas growth on urea was severely affected. Consistent with these findings, we found that Put2-HA was constitutively expressed in *gln3*Δ/Δ/ *gat1*Δ/Δ mutant grown in medium containing high levels of the preferred nitrogen source ammonium sulfate (Fig 5E). Our data indicate that in *C. albicans* proline utilization is not subject to NCR, a conclusion aligned with recently published transcriptome analyses [52].

In total, the data are consistent with mitochondrial metabolism and respiration being required to generate the signals responsible for amino acid-induced morphogenesis. The ability to optimally catabolize amino acids as sole nitrogen and carbon sources account for the concomitant increase in ATP. To critically test this notion, we examined whether mitochondria-derived ATP acts epistatic to Ras1/cAMP/PKA signaling. Consistent with Grahl et al. [14], colonies derived from a strain carrying the $RAS1^{G13V}$ allele, encoding a hyperactive mutant form of Ras1, exhibited filamentous growth in the presence of MB (S7B Fig), clearly indicating that Ras1 acts downstream of the mitochondria-derived metabolic signal.

Proline induces hyphal growth within phagosomes and enables *C. albicans* to escape from engulfing macrophages

We sought to place our novel insights regarding the critical role of proline metabolism in the induction of hyphal growth in a broader biological context and tested whether proline catabolism affects the capacity of *C. albicans* cells to form hyphae within macrophages and escape killing. First, using indirect immunofluorescence microscopy we examined whether Put2-HA is expressed in *C. albicans* cells engulfed by murine RAW264.7 macrophages (Fig 6A). *C. albicans* CFG185 (*PUT2/PUT2-HA*) cells were co-cultured with macrophages (MOI of 5:1; C:M) for 90 min. Strain CFG185 exhibits activation of proline catabolism in the presence of arginine, ornithine, and proline (Fig 4E). The macrophages were imaged using antibodies against the HA tag (1˚, rat anti-HA; 2˚, goat anti-rat antibody conjugated to Alexa Fluor 555) and LAMP-1, a lysosomal marker that is enriched in phagosomes. Confocal images clearly showed that *C. albicans* cells engulfed by macrophages express Put2, and that the Put2 expressing fungal cells are localized to Lamp1 compartments (see the orthogonal view of merged channels, lower left panel). The results indicate that *C. albicans* cells within macrophage phagosomes express Put2.

Next, we assessed the importance of the proline catabolic pathway components to escape macrophages. To facilitate comparisons with results obtained in other laboratories, we repeated the construction of the proline catabolic pathway mutations in the SC5314 strain background; strains lacking *PUT1*, *PUT2*, *PUT3* or both *PUT1* and *PUT2* were constructed using CRISPR/Cas9. The full genome of each mutant strain was sequenced; the sequence coverage varied from 42—65X and after assembly the contig coverage accounted for ≥98 of the reference SC5314 genome (Assembly 22, version s06-m01-r01; [58]). Each strain was found to carry the intended null mutation in the correct chromosomal locus and no large dissimilarities to the reference genome or off-target mutations were evident. Furthermore, no phenotypic differences were detected in comparison to the PMRCA18-derived strains.

As expected, SC5314 (WT) and CRISPR/Cas9 control strains (pV1093 and pV1524), lacking guide sequences to target Cas9, exhibited robust hyphal growth when co-cultured with RAW264.7 macrophages (Fig 6B). By contrast, and similar to heat killed SC5314, the strains carrying *put1*-/-, *put2*-/-, *put3*-/- and *put1*-/- *put2*-/- mutations were unable to efficiently form filaments from within engulfing macrophages (Fig 6B). As hyphal formation enables *C. albicans* cells to escape macrophages and thereby facilitates survival, we analyzed the candidacidal activity of macrophages by assessing fungal cell viability by assessing colony forming units

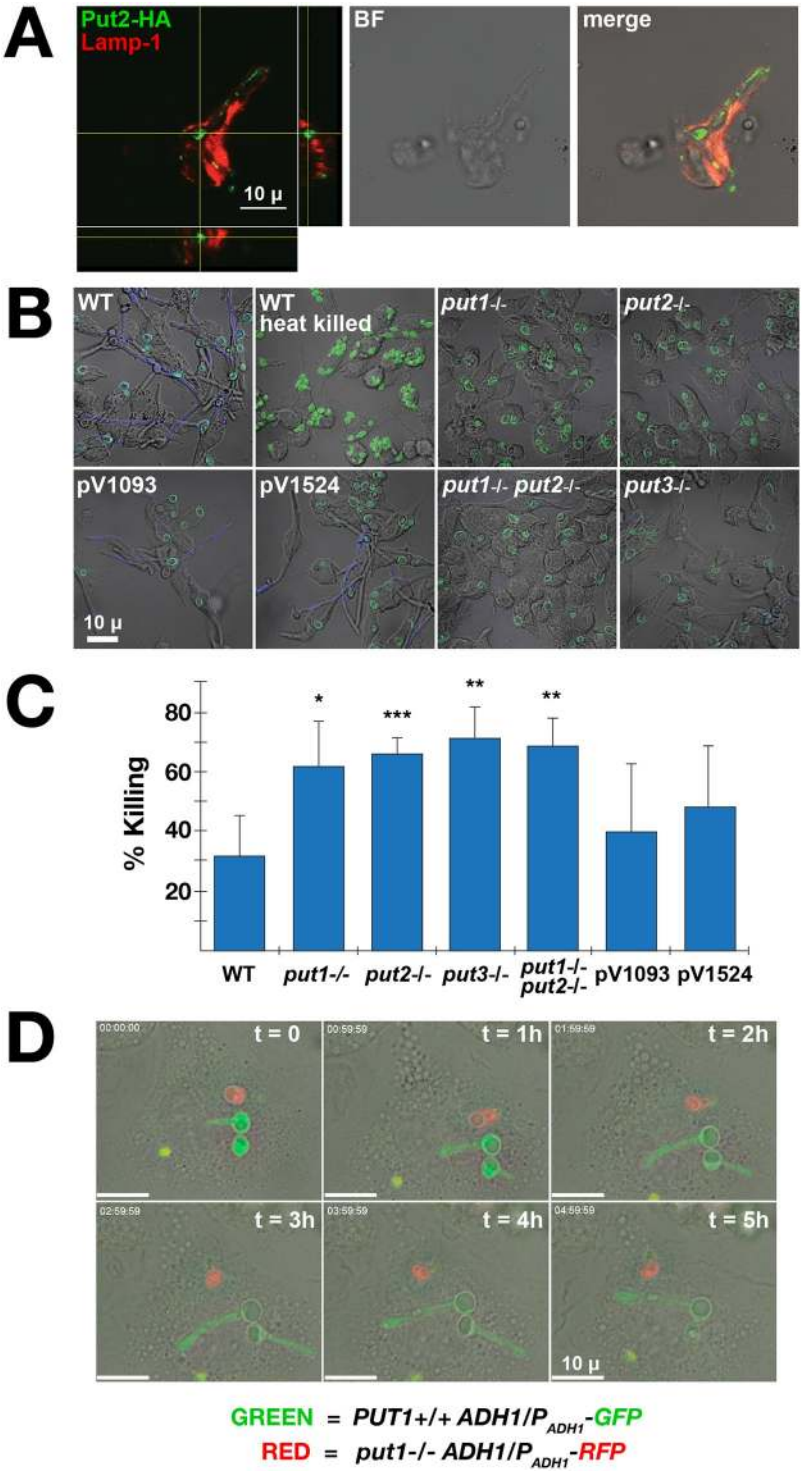

Fig 6. Mitochondrial proline catabolism is required by *C. albicans* cells to escape murine macrophages. A. Confocal immunofluorescence microscopy of *C. albicans* cells expressing Put2-HA (CFG185) in the phagosomes of RAW264.7 macrophages. Primary antibodies (rat anti-HA and rabbit anti-Lamp1) and secondary antibodies (Alexa Fluor 555 conjugated goat anti-rat antibody and Alexa Fluor 488 conjugated goat anti-rabbit) were used to visualize Put2 and the lysosomal compartment, respectively. Orthogonal view of merged channels is shown in the lower right panel. Scale bar = 10 µ. **B.** Proline catabolism is required for hyphal growth of *C. albicans* in macrophages. Wildtype (WT; SC5314), heat killed WT, *put1-/-* (CFG139), *put2-/-* (CFG207), *put3-/-* (CFG146), *put1-/- put2-/-* (CFG159) and CRISPR/Cas9 control strains CFG181 (pV1093) and CFG182 (pV1524) pre-grown in YPD and stained with FITC

were co-cultured with RAW264.7 macrophages at a MOI of 3:1 (C:M). After 30 min, external non-phagocytosed cells were removed by washing, and the co-cultures were incubated an additional 4 h. External (escaping) hyphal cells were stained with calcofluor white (CFW). Scale bar = 10 μ. **C**. Macrophage killing of *C. albican*s. Strains as in **B** (not stained) were co-cultured with RAW264.7 at a MOI of 3:1 (C:M) for 3 h. After lysing macrophages, viability of *C. albicans* was assessed by quantitating the number of CFU. The percent killing was determined by comparison to the viability of cells grown in the absence of macrophages. **D**. *put1-/-* mutant is unable to escape the phagosome of primary BMDM. The growth and morphogenesis of wildtype (Green, *ADH1/*P_{ADH1}*-GFP*) and *put1-/-* (Red, *ADH1/*P_{ADH1}*-RFP*) cells phagocytosed in the same primary BMDM was monitored by time-lapse microscopy for 5 h.

https://doi.org/10.1371/journal.pgen.1007976.g006

(CFU). Consistent with our microscopic analysis, in comparison to wildtype cells, the proline mutants were killed more efficiently (Fig 6C). Together, these results indicate that *C. albicans* cells rely on proline catabolism to induce hyphal growth in phagosomes, a response that facilitates escape from killing by macrophages.

We carried out time lapse microscopy (TLM) to visualize growth of *C. albicans* cells within phagosomes of engulfing macrophages. Wildtype and *put1-/-* stains, constitutively expressing GFP (*ADH1/*P_{ADH1}-GFP) and RFP (*ADH1/*P_{ADH1}-RFP), respectively, were co-cultured together with bone marrow-derived macrophage (BMDM) for 30 min before washing off non-phagocytosed external fungal cells. As expected, the GFP expressing wildtype cells robustly formed hyphae in the phagosome. By contrast, RFP expressing *put1-/-* mutant did not form hypha or grow. The result confirms that proline catabolism is required for growth and escape of *C. albicans* cells from macrophage phagosomes.

Discussion

In this study we have found that ATP generating mitochondrial proline catabolism is required to induce hyphal development of *C. albicans* cells in phagosomes of engulfing macrophages. The finding that proline catabolism, also required for the utilization of arginine and ornithine, is required to sustain the energy demands of hyphal growth provides the basis to understand the central role of mitochondria in fungal virulence. The energy status of the fungal cell is clearly a key signal that engages the genetic programs underlying yeast-to-hyphal transitions. The dependence on the energy producing proline catabolic pathway to induce *C. albicans* cells to switch morphologies is instrumental in their ability to escape from macrophages. Our results are consistent with a recent model postulating that elevated cellular levels of ATP induces hyphal morphogenesis [14] and with early reports that amino acid catabolism promotes filamentous growth [12, 13, 59]. Our experimental findings are schematically summarized in Fig 7.

Our work provides a framework to integrate several fragmentary observations regarding amino acid-induced morphogenesis. For example, Land et al. [11, 12] observed that the most potent morphogenic amino acids arginine and proline are those metabolized to glutamate. Our results show that this occurs strictly via the mitochondrial localized proline utilization pathway essentially as described in *S. cerevisiae* [60–62] with the exception that proline metabolism is not under nitrogen regulation (Fig 5E, [52]). Consistently, ornithine, an intermediate in arginine catabolism, also acts as a potent inducer of morphogenesis (Fig 1A; [12, 59]). Glutamate is further converted to α-ketoglutarate, an intermediate in the TCA cycle. These metabolic reactions are coupled to the generation of reduced electron carriers $FADH_2$ and NADH, which are oxidized in the mitochondria powering ATP synthesis. Amino acid induction of hyphal growth exhibits a strict requirement for Ras1 (Fig 2B) and cells grown in the presence of these inducing amino acids have high levels of active Ras1 (Fig 2C) and elevated levels of intracellular ATP (Fig 3A). The metabolic inhibitors nor-NOHA (Car1) and L-THFA (Put1) and methylene blue (MB, an uncoupler of mitochondrial respiration, block the induction of

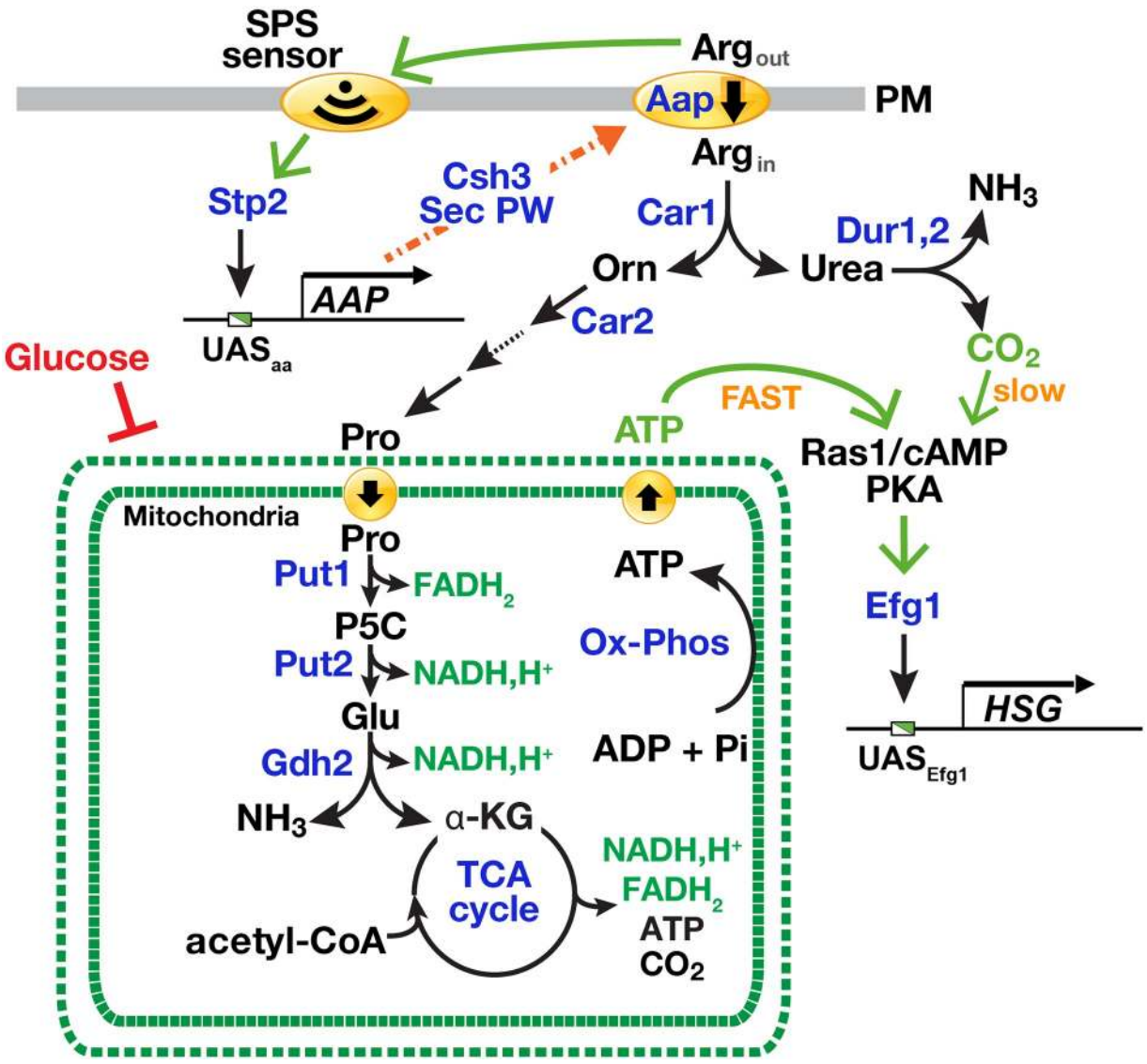

Fig 7. Arginine induces morphogenesis in *C. albicans* through mitochondria-dependent activation of Ras1/cAMP/PKA pathway. The presence of extracellular arginine enhances arginine uptake by binding to the SPS-sensor, leading to the endoproteolytic activation of transcription factor Stp2. The active form of Stp2 efficiently targets to the nucleus and binds the UAS_{aa} in the promoter of genes encoding amino acid permeases (*AAP*). Amino acid permeases are cotranslationally inserted into the membrane of the ER, and transported to the plasma membrane (PM, arrow) via the secretory pathway, a process that requires the ER membrane-localized chaperone Csh3. The increased functional expression of amino acid permeases (Aap) lead to an enhanced capacity to take up arginine. Intracellular arginine is catabolized by arginase (Car1) yielding ornithine and urea. Urea is further degraded by the urea amidolyase (Dur1,2) generating CO_2 and NH_3. Ornithine is further catabolized to proline in the cytoplasm in a series of enzymatic reactions starting with the ornithine aminotransferase (Car2). Proline is transported into the mitochondria where it is catabolized by Put1 and Put2 forming glutamate. These reactions generate the reduced electron carriers $FADH_2$ and $NADH,H^+$, respectively. Glutamate is oxidized by glutamate dehydrogenase (Gdh2) forming α-ketoglutarate in a reaction that liberates NH_3 and generates $NADH,H^+$. α-ketoglutarate feeds directly into the mitochondrial-localized TCA cycle. The reduced electron carriers generated by proline, glutamate and TCA cycle metabolic events are oxidized in reactions coupled to the generation ATP by mitochondrial oxidative phosphorylation. The elevated levels of ATP in the cytoplasm activate the adenyl cyclase (Cyr1) in a Ras1-dependent manner, which activates the downstream protein kinase A (PKA) signaling pathway and the effector transcription factor Efg1. The active phosphorylated form of Efg1 binds the UAS_{Efg1} in the promoter of hyphal specific genes (*HSG*), thereby inducing yeast-to-hyphal morphogenesis. The catabolism of arginine via the proline pathway induces hyphal growth more rapidly (FAST) than the Dur1,2 generated CO_2 (slow). Mitochondrial activity is repressed in the presence of high glucose.

https://doi.org/10.1371/journal.pgen.1007976.g007

filamentation (Figs 2D, 2E and 3B). Our analysis demonstrates that arginine and proline induce morphogenesis by virtue of a shared metabolic pathway (Fig 4C–4F).

Together, our findings are well aligned to the recent model proposed by Grahl et al. [14], where mitochondrial ATP synthesis facilitates Ras1 activation in cooperation with the adenylate cyclase (Cyr1) leading to increased cAMP production and to activation of the Efg1 transcription factor. The finding that arginine-induced hyphal growth occurs rapidly (Fig 4G), suggests that a brief exposure to arginine may suffice to trigger filamentous growth. According to Grahl et al. (2015), Ras1 activation by ATP appears to be independent of the AMP kinase, a key regulator of cellular energy homeostasis. The ATP-binding pocket within the active site of mammalian adenylyl cyclase has been shown to act as an ATP sensor [63]. Although it has been proposed that Cyr1 may function similarly as an ATP sensor this has yet to be confirmed in *C. albicans*. Regardless of the mechanism, exceeding a critical threshold of ATP is likely required to induce cAMP synthesis. It is known that the cAMP produced by Cyr1 does not necessarily correlate to the strength of the inducer and that transient short-lived spikes in cAMP are sufficient to trigger phosphorylation and eventually activation of Efg1 [29]. Consequently, spikes of ATP transiently generated by proline catabolism may efficiently induce hyphal specific genes (*HSG*).

We have clearly shown that arginine-, ornithine- and proline-induced hyphal growth is dependent on Ras1, which is not accounted for by other models of amino acid-induced morphogenesis (reviewed in [4, 7], despite the fact that Ras1 is known to be important in induction of filamentous growth in the presence of amino acid-rich serum [24]. Both the presumed amino acid sensing Gpr1-Gpa2 pathway [64, 65] and the Dur1,2-dependent CO_2 model for arginine-induced morphogenesis [32] are thought to bypass Ras1 and involve direct interactions with adenylyl cyclase (Cyr1). Also, contrary to the previous report [32], CO_2 generated by the Dur1,2-dependent catabolism of urea is not the primary morphogenic signal. Specifically, induction of filamentous growth in the presence of arginine or proline as sole nitrogen source proceeds more quickly than that observed by the metabolism of urea (Fig 4G). In addition, *DUR1,2* expression is tightly regulated by NCR, i.e., in the presence of ammonia, urea metabolism is repressed [57]. By contrast, the conversion of arginine to proline is not under NCR control (Fig 5E, [52]). Finally, when cells were shifted from YPD to medium containing arginine as sole carbon and nitrogen source, proline catabolic genes (*PUT1* and *PUT2*) were derepressed much faster than *DUR1,2* (Fig 4C), indicating that arginine is rapidly converted to proline. We have noted that the constitutive expression of arginase represents a common and undesired technical problem in proteomic analyses using SILAC (Stable Isotope Labeling by/with Amino acids in Cell culture) due to the rapid conversion of arginine to proline in eukaryotes [66–69]. In *Schizosaccharomyces pombe*, the deletion of two arginase genes (one a *CAR1* homologue) and the single ornithine transaminase (*CAR2* homologue) rectified this problem [66]. We predict, that similar deletions would be helpful in the quantitative analysis of the *C. albicans* proteome.

Earlier reports by Nickerson and Edwards [70] and Land et al. [11] suggested that mitochondrial activity is repressed during filamentous growth. By contrast, other more recent work has shown that hyphal formation occurs predominantly under aerobic conditions [17] and is associated with increased respiratory activity [14, 15]. Based on our findings (Fig 5C), the seemingly conflicting observations could be explained if, as in *S. cerevisiae*, the synthesis of mitochondrial respiratory enzymes are subject to glucose repression [71, 72]. There is surprisingly little information available regarding glucose repression of mitochondrial function in *C. albicans*, and whether the regulatory circuits are wired similar to those in *S. cerevisiae*. However, we note that Land et al. [11] used growth conditions with high glucose (1.8%; 100 mM), whereas studies by [14, 15] were carried out using low glucose (10 mM, i.e., $\approx$ 0.2%).

In striking contrast to the current view that *C. albicans* mitochondrial function is insensitive to glucose repression [73–75], our results clearly demonstrate that glucose represses respiration in the presence of proline (S6 Fig). Cells grown aerobically in high glucose exhibit fermentative metabolism (Fig 5C), i.e., the well-characterized Crabtree effect [76]. In glycolysis, conversion of glucose to pyruvate is coupled to reduction of NAD^+ and to the generation of ATP. Only small amounts of the cofactor is available in the cytosol. Consequently, when mitochondrial functions are glucose repressed, cells use fermentation to oxidize NADH and regenerate NAD^+, thereby enabling cytoplasmic ATP synthesis to continue. Under conditions when proline is the sole nitrogen source and high glucose is present, cells use glucose for energy and as carbon-source, whereas proline catabolism merely supplies cells with nitrogen, i.e., proline utilization is low (Fig 5B). However, when glucose becomes limiting (<0.2%), the respiratory capacity of mitochondria increases (S6 Fig), enabling cells to efficiently oxidize NADH and generate ATP by oxidative phosphorylation; under these conditions, cells use proline for energy and as the carbon- and nitrogen-source, i.e., proline utilization is high (Fig 5B). Together our results show that proline metabolism is a sensitive indicator of mitochondrial function in *C. albicans*.

Our observation that high glucose represses mitochondrial function, provides a mechanistic understanding of how high glucose inhibits hyphal morphogenesis [13, 33]. Cells grown on 2% glucose have elevated levels of reduced cofactors, such as NADH (Fig 5A), suggesting that the capacity of mitochondria to oxidize NADH is suboptimal, i.e., the cellular capacity to regenerate NAD^+ is rate limiting, a phenomenon termed over-flow metabolism [54]. It is important to note that, based on the *S. cerevisiae* paradigm, the pyruvate formed in glycolysis needs to be converted to acetyl-CoA to prime the TCA cycle. The mitochondrial-localized pyruvate dehydrogenase complex is predominantly responsible for the conversion of pyruvate to acetyl-CoA during glucose-limited, respiratory growth [71, 72]. Indeed, pharmacological inhibition of glycolysis has been shown to arrest filamentous growth of *C. albicans* even in the presence of proline [11]. Alternatively, β-oxidation of lipids may contribute the necessary acetyl-CoA [9].

We have placed the SPS sensing pathway, the primary sensing system of extracellular amino acids, in context to the major intracellular signaling pathways governing in nutrient regulated morphogenesis. SPS-sensor initiated signals do not directly induce hyphal growth, but rather facilitate morphogenesis by up-regulating the capacity of cells to take up inducing amino acids (Fig 7). Experimental support for this conclusion includes the following observations. First, amino acid-induced activation of SPS-sensor signaling does not strictly correlate with the induction of filamentous growth (Fig 1A). Second, the inability of a *ssy1* null mutant to undergo morphogenesis can be rescued by expressing a constitutively active form of Stp2 (*STP2**) but not Stp1 (*STP1**). Stp2 is the effector transcription factor that controls amino acid permease gene expression, whereas Stp1 activates the expression of secreted aspartyl proteases and oligopeptide transporters [36]. Consistently, and similar to Kraidlova et al. [77], we found that the expression of six *C. albicans* orthologues (*GAP1-GAP6*) of the *S. cerevisiae* general amino acid permease (*GAP1*) are regulated by the SPS sensing system, perhaps with the exception of *GAP4* expression, which is comparatively expressed at very low levels. Third, filamentous growth is dependent on amino acid catabolism. The weak filamentation observed in the *csh3*Δ/Δ mutant grown in 10 mM proline can be attributed to the residual uptake of proline as previously described [37]; apparently, the residual systems are expressed and function at high extracellular concentrations of proline [59, 78]. Thus, the filamentous growth defect observed in cells lacking a functional SPS sensing pathway, i.e., *SSY1* or *CSH3* null mutants, is due to the inability to efficiently take up inducing amino acids from the extracellular environment, a requisite for their metabolism [37, 38].

Together our findings have important implications on understanding how *C. albicans* cells interact with host immune cells. Transcriptomic studies examining macrophage-*C. albicans* interactions by Lorenz et al. [9] showed that arginine biosynthesis genes are peculiarly upregulated in phagocytosed cells. Furthermore, the results suggest that the phagosome is likely a glucose-poor environment as an increased expression of genes that favor gluconeogenesis and mitochondrial function was also noted [9]. Interestingly, arginine utilization appears to proceed concomitant with arginine biosynthesis as deduced from the increased arginase transcripts in phagocytosed cells [9, 32]. In a follow-up study, the apparent upregulation of arginine biosynthesis was suggested to be a response to the macrophage oxidative burst [79]. Interestingly, the expression of *DUR1,2* in phagocytosed cells was not significantly altered. Our finding that the enzymes responsible for proline utilization are upregulated indicates that proline is either made available by the host or is the result of arginine catabolism.

In the light of these results, the challenging question is where the hyphae inducing amino acids come from, from the macrophage or from nutrients stored within *C. albicans* cells prior to their being phagocytosed. In *S. cerevisiae*, > 90% of free arginine is sequestered in the vacuole and the non-compartmentalized and cytosolic arginine is catabolized by arginase [80]. Given that arginine is catabolized to proline via the arginase pathway with ornithine acting as a transitory intermediate, it is possible that vacuolar stores of arginine are activated in the phagosome to support the demand for cellular energy. When glucose becomes limiting, *C. albicans* may rely on the catabolism of amino acids, particularly proline, as primary energy. This is reminiscent of the requirement of proline catabolism for Trypanosome survival in the Tsetse fly vector [81–84].

Proline-induced morphogenesis is repressed under acidic conditions [13, 59], presumably a condition confronting newly phagocytized *C. albicans* cells. This raises the interesting conundrum as to how *C. albicans* cells deal with this environmental challenge and filament. It is possible that Stp2-mediated alkalization of the phagosome reported by Vylkova and Lorentz [85] is a key predisposing event that facilitates proline-induced morphogenesis. We found that alkalization is not Dur1,2-dependent (Fig 4D), indicating that an alternative mechanism triggers alkalization. Accordingly, the Stp2-dependent induction of arginine uptake and its subsequent Put1- and Put2-dependent metabolism generates glutamate, which is deaminated to α-ketoglutarate by glutamate dehydrogenase (Gdh2) (Fig 7). The resulting NH_3 may provide the explanation for the observed alkalization. As already pointed out, the source of amino acids in the macrophage phagosome remains a very interesting question. Numerous metabolic signatures appear to reflect a microenvironment with a poor nitrogen content. For example, based on the transcriptional analysis of the *C. albicans*-macrophage interaction, *OPT1*, encoding an oligopeptide transporter, is upregulated in phagocytosed cells [9]. *OPT1* expression is controlled by the SPS-sensor signaling and the downstream transcription factor Stp1 [36, 39]. *STP1* expression is itself under tight NCR control [39]. Thus, the upregulated expression of *OPT1* strongly suggests that NCR is relieved in phagocytosed cells and that sufficient levels of amino acids are present to induce the SPS-sensor. As to the origin of amino acids in the phagosome, *C. albicans* may excrete amino acids liberated from storage compartments, loaded during growth in rich media. In *S. cerevisiae*, under defined conditions, amino acids are known to be excreted at detectable levels [86] and under certain circumstances activate SPS-sensor signaling [87]. Thus, amino acids may provide an autocrine function to induce filamentous growth of phagocytosed *C. albicans* cells.

The results presented here provide a clear example of how *C. albicans* cells sense and respond to nutrients present in the host to ensure proper nutrient uptake and continued survival. The molecular components underlying nutrient uptake are often referred to as virulence factors. When afforded the opportunity, *C. albicans* will alter developmental programs to

optimize nutrient uptake systems that enable the better exploit host environments and to evade the primary immune response [3, 88, 89]. The identification and understanding of fungal virulence factors is necessary to therapeutically disturb their function upon infectious growth and thereby facilitate the ability of host immune systems to re-establish and maintain the integrity of the host. We are excited by the prospect of exploiting mitochondrial proline metabolism to probe the nutrient environment of the macrophage phagosome, a currently poorly characterized environment.

Materials and methods

Strains, media and chemicals

C. albicans strains and primers used are listed in Supporting Information, S1 Text (S1 Table) and S2 Text (S2 Table), respectively. All strains were cultivated in YPD medium (1% yeast extract, 2% peptone, 2% glucose) at 30 ˚C. Minimal synthetic dextrose (SD) medium containing 0.17% YNB (Yeast Nitrogen Base without amino acids and without ammonium sulfate; Difco), 2% glucose, and 5 g/l ammonium sulfate (≈ 38 mM) was used as indicated. Media were made solid by 2% (w/v) Bacto agar. Where appropriate, 200, 100 or 25 μg/ml nourseothricin (Nou; Jena Biosciences, Jena, Germany) was added to the medium. The ability of amino acids to induce filamentous growth was determined on buffered solid synthetic (SXD) media containing 0.17% YNB, 2% glucose, and 10 mM of the indicated amino acid (X) as sole nitrogen source, or at concentrations as described in the figure legends. Fifty mM 2-(N-morpholino) ethanesulfonic acid (MES) was included in media and the pH was adjusted to 6.0 using NaOH. To minimize residual nitrogen, the SXD media were made solid using 2% (w/v) highly purified agar (Biolife, Milano, Italy). Where indicated 0.2% glucose, 1% lactate or 1% glycerol replaced 2% glucose as carbon source. The following media were used to screen CRISPR/Cas9-derived knockout phenotypes: YPD-MM; SUD; SPD; and YNB+Arg+BCP. YPD-MM is standard YPD supplemented with 1.5 mg/ml MM (2-([(([(4-methoxy-6-methyl)-1,3,5-triazin-2-yl]-amino)carbonyl)amino]-sulfonyl)-benzoic acid; Dupont Ally); SUD and SPD were prepared as SXD containing urea (U), or proline (P) as sole nitrogen source; YNB +Arg+BCP contains 0.17% YNB, 10 mM arginine (Arg) as sole nitrogen and carbon source, and 0.03 μg/mL bromocresol purple (BCP; Sigma) as indicator, with the pH adjusted to 4.0 using 1 M HCl. Growth in the presence of specific metabolic inhibitors was assessed on media containing nor-NOHA (N-hydroxy-nor-L-arginine; BioNordika AB, Sweden) prepared in 100% dimethyl sulfoxide (DMSO) as 56 mM concentrated stock; a 26 mM working stock was prepared freshly diluting in ddH_2O. L-tetrahydro-2-furoic acid (L-THFA; Sigma) and methylene blue (MB; Sigma), were freshly prepared in ddH_2O as 1 M and 3 mM stocks, respectively. *Escherichia coli* strain DH10B was used for the construction of plasmids; LB medium supplemented where required with carbenicillin (Cb, 50 μg/ml), Nou (50 μg/ml), and/or chloramphenicol (Cm, 30 μg/ml). LB was made solid by 1.5% Bacto agar. Liquid cultures were grown with agitation at 150–200 rpm. The density of yeast suspensions was determined and adjusted (1 OD_{600} = 3 x 10^7 CFU/ml) [90]. Sterile Milli-Q ddH_2O was used in all experiments.

CRISPR/Cas9 mediated gene inactivation and reporter strain construction

The CRISPR/Cas9 gene editing was used to inactivate both alleles of *SSY1* (C2_04060C), *CSH3* (C4_03390W), *CAR1* (C5_04490C), *PUT1* (C5_02600W), *DUR1,2* (C1_04660W), *IRA2* (C1_12450C), *PUT1* (C5_02600W), *PUT2* (C5_04880C) or *PUT3* (C1_07020C). Sequences of synthetic guide RNAs (sgRNAs), repair templates, and verification primers are listed in S2 Text (S2 Table). The solo system plasmids pV1093 or pV1524 were used [91, 92]. These plasmids contain a cassette comprised of the *Candida*/*Saccharomyces* codon-optimized *CAS9*

endonuclease gene, *NAT* gene (recyclable in pV1524), sgRNA cloning site, and flanking sequences for genomic integration. For pV1093 and its derivative plasmids, the cassettes were integrated in an *ENO1* locus, whereas pV1524 and its derivatives were integrated in the *NEUT5* locus. The sgRNAs were designed as described [93] and were inserted in pV1093 or pV1524 by linker ligation. To summarize, oligo pairs p43/p44 (*SSY1*), p49/p50 (*CSH3*), p55/p56 (*CAR1*), p61/p62 (*DUR1,2*), p67/p68 (*IRA2*), p73/p74 (*PUT1*), p79/p80 (*PUT2*), and p85/p86 (*PUT3*), were separately phosphorylated and annealed prior to ligating them to dephosphorylated *Esp*3I (*Bsm*BI)-digested pV1093 or pV1524. Ligation reactions were purified and introduced into *E. coli* by electroporation. Transformants were selected on solid LB+Cb (or +Nou for pV1524 cloning) incubated overnight at 37 ˚C. Plasmids were sequenced using primer p91 (FS95). Plasmids (3 to 6 μg) containing the 20-bp sgRNA for *SSY1* (pFS013), *CSH3* (pFS017), *CAR1* (pFS024), *DUR1,2* (pFS039), *IRA2* (pFS028), *PUT1* (pFS080, pV1093 derivative), *PUT1* (pFS088, pV1524 derivative), *PUT2* (pFS083) and *PUT3* (pFS084) were digested with *Kpn*I and *Sac*I to release the cassette. Repair templates (RT) containing stop codon and specific restriction site were produced by template-less PCR using oligo pairs p45/p46 (*SSY1*), p51/p52 (*CSH3*), p57/p58 (*CAR1*), p63/p64 (*DUR1,2*), p69/p70 (*IRA2*), p75/p76 (*PUT1*), p81/p82 (*PUT2*), and p87/p88 (*PUT3*). For the creation of *ras1-/-* and $RAS1^{G13V}$ mutants, plasmid pV1121 (recreated using primers p98/p99 sgRNAs (*RAS1*)) and RT (p94/p95 (*RAS1*) and p92/p93 ($RAS1^{G13V}$)) from Vyas et al. (2015) were used. PCR-purified digested plasmid and repair templates were co-transformed into *C. albicans* cells (PMRCA18 or SC5314 background) at a 1:3 ratio (w/w, plasmid:repair template). The hybrid lithium acetate/DTT-electroporation method, with minor modifications, was used for transforming *C. albicans* [94]. After applying 1.5 kV of electric pulse, cells were recovered in YPD medium supplemented with 1 M sorbitol for at least 4 h and then plated on YPD+Nou plates; Nou^R colonies were selected 2 days after plating. Nou^R transformants were pre-screened according to the expected phenotype prior to PCR and restriction analysis using primers and restriction enzymes indicated in S3 Fig and S2 Text (S2 Table).

Strain CFG240 (*put1-/-*) expressing P_{ADH1}-*RFP* was constructed as follows. Strain CFG139 (*put1-/-*) is Nou resistant (Nou^R) due to a CRISPR/Cas9 cassette integrated in *NEUT5*. CFG139 was grown in YP + 2% maltose, the Nou sensitive (Nou^S) strain CFG155 was isolated as a colony exhibiting reduced growth on YPD supplemented with 25 μg/ml Nou. CFG155 was transformed with *Kpn*I- and *Sac*I-digested pJA21 (P_{ADH1}-*RFP*) [95]. RFP-positive clones were verified by PCR (p112/p113). SC5314 derived strains expressing C-terminal HA tagged Put2 were constructed by transforming a 4.8 kb epitope-tagging cassette amplified using primers p108/p109 and plasmid pFA6a-3HA-SAT1 as template (generous gift from Karl Kuchler). Nou^R transformants were screened by colony PCR using primers p110/p111 and verified by immunoblot analysis.

Full genome shotgun sequencing

Genomic DNA was isolated from *put1-/-* (CFG139), *put2-/-* (CFG207), *put3-/-* (CFG146), *put1-/- put2-/-* (CFG159) and CRISPR/Cas9 control strains CFG181 (pV1093) and CFG182 (pV1524) and sequenced. Prior to library construction, extracted DNA was purified with Agencourt AMPure XP beads (Beckman Coulter, USA) in order to remove short sequences (<100 bp). Aliquots (25 μl) of DNA were mixed with 45 μl of AMPure beads with a ratio of 1:1.8 and incubated 15 min. Initial DNA concentrations following purification were evaluated using Quant-iT PicoGreen dsDNA Assay kit (ThermoFisher, USA). Absorbance was measured at 530 nm, using a Tecan Ultra 384 SpectroFluorometer (PerkinElmer, USA).

Library construction was carried out with the QIAGEN-FX kit (Qiagen, Germany) with a DNA input of 100 ng DNA per sample and a digestion time of 13 min without enhancer. Following fragmentation, adapter sequences were ligated, and ligated DNA fragments were amplified by 9 cycles of PCR and DNA was purified with AMPure XP beads. The quality of the library samples were evaluated with an Agilent Bioanalyzer using DNA1000 cartridges. The average length of the fragments excluding adapter sequences was 455 bp.

Prior to sequencing, the samples were denatured with 0.2 N NaOH. A final volume of 570 μl of pooled library was mixed with denatured Phix control (30 μl) and loaded on an Illumina Mi-Seq 2x300 flow-cell and reagent cartridge. De-multiplexing and removal of indexes and primers were done with the Illumina software v. 2.6.2.1 on the instrument according to the standard Illumina protocol. Initial de novo assembly of quality-controlled reads was done with SPADES v. 3.11.1 and standard settings [96]. Mapping of assembled contigs was done with Ragout v 2.0 [97] using Sibelia for synteny detection [98]. Visualization of results and generation of reports on the assembly quality and other factors were done with QUAST v. 4.6.1 [99].

NanoLuc transcription-translation reporter of SPS-sensor activation

The NanoLuc-PEST (Nlucp) construct was used to create the reporter of SPS-sensor dependent transcription (S2 Fig). The presence of PEST sequences ensures rapid degradation of NanoLuc luciferase, thereby enhancing sensitivity [41]. Up- and downstream regions of the *CAN1* ORF were amplified using genomic DNA from PMRCA18 as template and primers p100/p101 (0.9 kB upstream) and p104/p105 (0.98 kB downstream) (S2 Text). An approximately 0.7 kB Nlucp gene sequence was amplified from plasmid pCA873 [100] using primers p102/p103. These amplicons were digested with appropriate FastDigest enzymes (Thermo Scientific) and purified; i.e., the *CAN1* upstream amplicon was digested with *Kpn*I/*Xho*I, the *CAN1* downstream with *Xba*I/*Not*I, and Nlucp DNA fragment with *Xho*I/*BamH*I. Using T4 DNA Ligase (Thermo Scientific), the upstream fragment was first ligated to *Kpn*I/*Xho*I-digested pSFS2a vector [94] creating pFS006. The purified Nlucp DNA was then ligated into *Xho*I/*BamH*I restricted pFS006 creating pFS007. Finally, the downstream fragment was ligated into *Xba*I/*Not*I restricted pFS007 creating pFS010. The plasmids were introduced into *E. coli* and transformants selected on LB+Cm+Nou plates incubated at 30 ˚C. The desired reporter construct, purified from *Kpn*I/*Not*I restricted pFS010, was introduced into *C. albicans* wildtype (PMRCA18) and SPS-deficient mutant strains (*ssy1*Δ/Δ, *ssy5*Δ/Δ, and *stp2*Δ/Δ) by electroporation. Selection was carried out on YPD+Nou and Nou^R clones carrying the integrated Nlucp construct were identified by PCR using primers p107/p106.

For analysis of amino acid-induced SPS-sensor activation, Nano-Glo Luciferase Assay System (Promega GmbH, Germany) was used following the manufacturer's protocol. Briefly, log phase SD cultures were first standardized to OD ≈ 0.8 before adding 50 μl of the cell suspension into each well of Nunc 96 well microplate (white). Then, cells were induced with 50 μM of the indicated amino acids for 2 h at 30 ˚C. Fifty microliters (50 μl) of Nano-Glo substrate diluted 1:50 in the supplied lysis buffer was added into each well of the microplate. After 3 min, bioluminescence was captured using microplate luminometer (Orion II, Berthold Technologies GmbH & Co. KG, Germany). Luminescence reading from treated wells were deducted from wells spiked with ddH_2O serving as uninduced control.

Filamentation assay

Solid filamentation assay was performed as described [14]. Briefly, cells from overnight YPD liquid cultures were harvested, washed once, and resuspended in sterile ddH_2O. The cell

density of cell suspensions was adjusted to $OD_{600} \approx 8$ before spotting 10 μl onto solid media. Plates were allowed to dry at room temperature before incubating at 37 ˚C as indicated to allow macrocolonies to form. Filamentation assays in the presence of metabolic inhibitors, nor-NOHA or L-THFA, were performed in a 6-well microplate format (~5 ml/well); otherwise, all assays were carried out using standard Petri plates (~35 ml/plate). For filamentation assays in liquid cultures, cells were washed and then adjusted to $OD_{600} \approx 25$. Cells were diluted in pre-warmed liquid medium at $OD_{600} \approx 0.5$ and then incubated at 37 ˚C with vigorous agitation for the specified time. Cell morphologies were assessed under epifluorescence microscopy using calcofluor white stain (CFW, Fluorescent Brightener 28, 1 mg/ml; Sigma).

qRT-PCR

Hyphal specific gene (HSG) expression in 24 h old macrocolonies was analyzed as follows: using a sterile glass slide, three to four macrocolonies of wildtype strain (PMRCA18) were collected by scraping and suspended in 1 ml of ice-cold PBS. Cells were harvested by centrifugation at 10,000 x g for 3 min (4 ˚C), snap frozen in liquid nitrogen and then stored at -80 ˚C until processed for RNA extraction. Gene expression in liquid grown cells was analyzed as follows: cells from overnight YPD cultures were harvested by centrifugation, washed and resuspended at an $OD_{600} \approx 25$ in pre-warmed liquid medium and incubated at 37 ˚C for 2- and 4-h before harvesting the cells by centrifugation; the cell pellets were snap frozen in liquid nitrogen. For arginine catabolic gene expression analysis, SC5314 was used as wildtype strain. Briefly, cells from log phase YPD culture growing at 30 ˚C were harvested, washed 3X with PBS, diluted in pre-warmed YNB+Arg medium (pH = 6.0, without BCP) at an $OD_{600} \approx 0.5$, and then incubated for 1 h at 37 ˚C under aeration. A portion of the washed cells were snap-frozen in liquid nitrogen to serve as reference (t = 0). Following 1 h incubation, cells in YNB +Arg were immediately harvested and then snap-frozen in liquid nitrogen for RNA extraction. To analyze the dependence of *GAP* genes expression to SPS pathway (i.e., Ssy1), wildtype (PMRCA18) and *ssy1*Δ/Δ (YJA64) cells were grown to log phase in SD medium at 30 ˚C before spiking with 1 mM of glutamine or ddH_2O for 30 min. Cells were collected from induced (glutamine) and non-induced (ddH_2O) cultures and snap-frozen in liquid nitrogen.

Total RNA was extracted from frozen cell pellets using RiboPure-Yeast Kit (Ambion, Life Technologies) essentially following the instructions of the supplier with the exception that cells were subjected to extra bead-beating step (Bio-Spec; 1 × 60 sec, 4 M/s). DNase-treated RNA extracts were reverse-transcribed using SuperScript III and Random Primers (Invitrogen, Life Technologies). cDNA preparations were diluted 1/40 in ddH_2O and 5 μl were used as template for qPCR using KAPA SYBR Green (Kapa Biosystems). Gene specific primers (500 nM) were added and reactions were performed in a Rotor-Gene 6000 (software version 1.7). The ΔΔCt method ($2^{-\Delta\Delta Ct}$) was used to quantitate the relative levels of gene expression. Levels of gene expression were normalized to *ACT1* or *RIP1* [101] as indicated.

ATP quantification

A bioluminescence-based ATP detection kit (Molecular Probes, Invitrogen) was used to quantify ATP levels in macrocolonies grown on SXD medium as indicated. ATP was extracted from eight, 24 h-old macrocolonies harvested using a sterile glass slide and then suspended in 1 ml sterile ice-cold Tris Buffered Saline (TBS; 50 mM Tris-Cl, pH 7.5, 150 mM NaCl). Cells were harvested at 10,000 x g for 3 min (4 ˚C) before re-suspending the entire pellet in TCA buffer containing 100 mM Tris-HCl (pH = 8.0), 10% trichloroacetic acid (TCA), 25 mM ammonium acetate, and 4 mM EDTA. Cell suspension was transferred to pre-chilled tubes containing glass beads and then subjected to bead beating (Bio-Spec; 5 × 1 min, 4 M/s with 2

min on ice between pulses). Cell lysates were collected and a portion of the supernatant was analyzed for ATP following the instruction of the manufacturer. Luminescence was analyzed using microplate reader (Berthhold) using 1 sec integration time. A portion of the same lysate was used to determine total protein concentration using the bicinchoninic acid (BCA; Sigma) assay. Results presented are average of ATP normalized to total protein concentration analyzed from 3 biological replicates; each replicate is an average of 2–3 technical replicates.

Immunoblotting

For Stp2 cleavage analysis, cells expressing Stp2-HA (PMRCA48) were grown to saturation in SD liquid medium overnight at 30 ˚C and then refreshed the following morning in 25 ml of fresh SD medium at a starting $OD_{600} \approx 0.3$. Cells were grown in a 30 ˚C-shaker to an OD_{600} of 1.5–2.2. For induction experiments, a 500-μl aliquot of log phase culture were separately added to tubes containing the indicated amount and type of amino acids or an equal volume of water for control, and then incubated for 5 min at 30 ˚C in a thermoblock shaking at 700 rpm. For Put2-HA expression analysis, cells from overnight YPD cultures were harvested, washed and then grown as indicated. Whole cell lysates were prepared using NaOH/TCA method as described previously with minor modifications [102]. Cells were lysed on ice with 280 μl of ice-cold 1.85 M NaOH with 7% ß-mercaptoethanol for 15 min; proteins were precipitated ON at 4 ˚C by adding the same volume of cold 50% TCA. Protein pellets were quickly washed with ice-cold 1 M Tris base (pH = 11) and then resuspended in 2X SDS sample buffer. In some instances, as indicated, due to highly variability in protein recovered from certain types of cells (i.e., yeast and filamentous forms) sample loading was normalized based on protein content. Samples were denatured in sample buffer at 95–100 ˚C for 5 min, the proteins were resolved in sodium dodecyl sulfate-polyacrylamide gel electrophoresis (SDS-PAGE) using 4–12% pre-cast gels (Invitrogen) and analyzed by immunoblotting on nitrocellulose membrane according to standard procedure. For Stp2-HA and Put-HA detection, HRP-conjugated anti-HA antibody (Pierce) was used at 1:2,500 dilution. For loading control, HRP-conjugated rat monoclonal α-tubulin antibody [YOL1/34] (Abcam) was used at 1:10,000 dilution. Membranes were blocked using TBST (TBS + 0.1% Tween) containing 10% skimmed milk; antibodies were diluted in TBST containing 5% skimmed milk. Immunoreactive bands were visualized by enhanced chemiluminescent detection system (SuperSignal Dura West Extended Duration Substrate; Pierce) using ChemiDoc MP system (Bio-Rad).

Active Ras1-Pull Down assay

Active Ras1 (Ras1-GTP) was analyzed in macrocolonies using Pierce Active Ras Pull-Down Kit (Thermo Scientific) following the manufacturer's instructions, but with an extra bead-beating step to ensure optimal disruption of cells. Five 24 h-old macrocolonies were scraped, pooled, and suspended in 1 ml ice-cold TBS in 2-ml microcentrifuge tubes (with caps). Cells were collected by centrifugation at 10,000 x g for 3 min (4 ˚C) and then resuspended in 400 μl of Lysis/Binding/Washing buffer (1X, Pierce kit) supplemented with protease cocktail (cØmplete mini, EDTA-free; Roche) and 1 mM PMSF. Pre-chilled glass beads were added, cell suspensions were subjected to multiple cycles of bead beating (6 × 40 sec, 4 M/s, 2 min on ice between pulses). After an initial clarification step at 1,000 rpm for 5 min, supernatants were collected and total protein was determined using the BCA assay. The concentration of protein in lysates was adjusted to 2 mg/ml using the lysis buffer as diluent and then 500 μg of protein was used for the immunoprecipitation. We used 12.5 μg protein for input and eluted bound protein in 25 μl. Proteins were resolved by SDS-PAGE and analyzed by immunoblotting. Total Ras and active Ras-GTP were probed with primary monoclonal anti-Ras clone X (1:300)

included in the kit, and secondary goat anti-mouse antibody (1:10,000; Pierce). For loading control, α-tubulin conjugated to HRP (1:10,000) was used. Membranes were blocked and the primary antibody diluted in TBST containing 3% BSA; the secondary and loading control antibodies were diluted in TBST containing 5% skimmed milk. Results presented are representative of at least 3 independent experiments.

Growth assays

For drop plates, cells from log phase YPD cultures grown at 30 ˚C were harvested, washed, and then adjusted to $OD_{600} \approx 1$. Five microliters of 10-fold serially diluted cell suspension were spotted onto the surface of the indicated SXD media and incubated at 30 ˚C for 2–3 days and photographed. For liquid assays, washed cells from log phase YPD cultures were diluted in the indicated SXD liquid medium to a starting $OD_{600} \approx 0.05$, and 300 μl were transferred into each well of a 10 x 10-well microplate and grown continuously for > 20 h at 30 ˚C with constant agitation. OD_{600} readouts were captured using BioScreen C MBR analyzer (Oy Growth Curves Ab Ltd, Helsinki, Finland).

Resazurin reduction assay

The membrane permeant, non-destructive redox indicator, Resazurin (Sigma), was used to measure the metabolic activity of intact cells growing in SXD. Briefly, reduction of the nonfluorescent resazurin dye by NADH or NADPH oxidoreductases in metabolically active cells generates the highly fluorescent resorufin which emits fluorescence at 590 nm [49]. Cells from overnight YPD cultures were harvested, washed once with sterile ddH_2O, and adjusted to $OD_{600} \approx 0.01$ (~3 x 10^5 CFU/ml) using the YNB-glucose base medium (~1.05x strength, pH = 6.0). Using a multi-channel pipette, 95 μl of this cell suspension were added to the well of a 96-well microplate followed by addition of 5 μl of 200 mM amino acid stock (10 mM final concentration). Plates were incubated at 37 ˚C for 2 h with agitation protected from light. After 2 h, 20 μl of filtered Resazurin dye (0.15 mg/ml) was added to each well and incubated for 2 h at 37 ˚C before measuring the fluorescence (560 nm excitation/590 nm emission) using EnSpire microplate reader (PerkinElmer).

TTC overlay assay

Macrocolonies grown on the indicated plates for 24 h were overlaid with 2 ml of molten TTC-agar solution (50–55 ˚C) containing 0.1% TTC (2,3,5 triphenyltetrazolium chloride; Sigma) dissolved in 67 mM potassium phosphate buffer (PPB, pH = 7.0) with 1% agar [15]. Plates were photographed 30 min after the overlaid solution became solid. The colorless TTC dye is cell permeant which can be reduced to the reddish 1,3,5-triphenylformazan (TTF) by NADH in the mitochondria [15, 48].

Extracellular oxygen consumption assay

Oxygen consumption assay was performed in *C. albicans* grown in synthetic proline medium containing the indicated carbon source (i.e., 2% glucose (SPD), 0.2% ($SPD_{0.2\%}$), or 1% glycerol (SPG) using the Extracellular Oxygen Consumption Assay (Abcam, ab197243) following manufacturer's protocol. Briefly, cells from log phase YPD culture were harvested, washed 3X with PBS, and then diluted in the indicated media at $OD_{600} \approx 0.3$. A 150 μl cell suspension was added into each well of a 96-well microplate with black walls and clear bottom. Ten microliters of Extracellular Oxygen Consumption Reagent, or medium (control), were added and the samples were mixed gently by moving the plate on a circular motion. FCCP (final conc.

10 μM) and antimycin (final conc. 10 μg/ml) were used as positive and negative controls, respectively. Plates were analyzed using Enspire microplate reader using Time Resolved Fluorescence (TRF). Signals were read every 90 sec for 120 repeats with optimal delay time of 30 μs and gate (integration) time of 100 μs. Signal from wells without cells were used as background signal.

Quantification of proline

The concentration of proline in media and in cell extracts was analyzed using the quantitative ninhydrin method [103]. Proline utilization was assessed as follows: cells grown overnight in YPD were washed and resuspended to an $OD_{600} \approx 0.5$ in pre-warmed synthetic proline media containing 10 mM of proline and the indicated carbon source. The cultures were incubated under constant aeration for 2 h at 37 ˚C, and the amount of proline in culture supernatants was analyzed. Proline utilization was defined by comparison to non-inoculated media.

C. albicans co-culture with murine macrophages

The murine macrophage cell line RAW264.7 (ATCC) was cultured and passaged in Dulbecco's modified Eagle's medium/high glucose (HyClone, GE Healthcare Life Sciences, Amersham, UK) supplemented with 10% fetal bovine serum, 100 U/ml penicillin and 100 μg/ml streptomycin (hereafter referred as D10) at 37˚C with 5% CO_2. Prior to co-culture with *C. albicans*, RAW264.7 cells (1 x 10^6) in D10 medium were seeded on a 24-well microplate containing sterile cover slips and were allowed to adhere overnight in a humidified chamber at 37˚C and 5% CO_2. Fungal cells (3 x 10^8) were harvested from overnight YPD cultures and stained with 1 mg/ml FITC solution in 0.1 M $NaHCO_3$ buffer (pH = 9.0) in the dark for 15 min at 30 ˚C. Cells were washed 3X with PBS before resuspending in equal volume of PBS. Fungal cells were added to macrophage at MOI of 3:1 (Candida:Macrophage, C:M) and were then allowed to interact for 30 min. Non-phagocytosed cells were removed by washing the cells at least 5X with pre-warmed Hank's Balanced Salt Solution (HBSS) and 1X with D10 medium. Cells were allowed to interact for an additional 4 h in fresh D10 medium before fixing with 3.7% formaldehyde-PBS for 15 min in the dark at room temperature. Fixed cells were then washed 3X with PBS before staining with calcofluor white (10 μg/ml) for 1 min. After 2X PBS washing, coverslips were mounted on glass slides using ProLong Gold antifade reagent (Invitrogen). Images were obtained using LSM 800, 63x/1.2 oil.

C. albicans killing by murine macrophages

The survival of *C. albicans* co-cultured with macrophages was assessed by colony forming units (CFU) essentially as described [104]. Briefly, RAW264.7 cells in D10 were seeded into a 96-well microplate at a density of 1 x 10^5 per 200 μl and allowed to adhere overnight. *C. albicans* cells from overnight YPD cultures were processed without staining and added at a MOI of 3:1 (C:M). The co-cultures were incubated for 3 h prior to assessing fungal cell viability by CFU; each well was treated to final concentration of 0.1% Triton X-100 for 2 min to lyse macrophage and serial dilutions were prepared and plated onto YPD. CFUs were counted 2 days after incubation at 30 ˚C. The ability of macrophages to kill *C. albicans* (% killing) was determined by comparison of fungal CFU recovered in the absence of macrophages.

Indirect immunofluorescence microscopy of phagocytosed *C. albicans*

RAW264.7 cells were co-cultured with *C. albicans* cells, CFG185 (*PUT2/PUT2-HA*), for 90 min on glass coverslips at a MOI of 5:1 (C:M). Cells were fixed in 3.7% formaldehyde-PBS for

15 min, and permeabilized in 0.25% Tween-20 for 15 min, both incubations were at room temperature. The fixed and permeabilized cells were incubated in zymolyase buffer (2U zymolyase 100T (Zymo Research, Irvine, CA, USA), 10 mM DTT in PBS) for 1 h at 30 ˚C. After washing, cells were incubated at room temperature in 0.25% Tween-20 for 10 min and blocked in 5% FBS for 30 min. Cells were incubated overnight at 4 ˚C with rat anti-HA (Roche, Germany, #1867423) and rabbit anti-Lamp1 (Abcam, UK, #ab24170) primary antibodies diluted 1:500 in 0.25% Tween-20. Cells were washed with PBS and incubated 2 h with Alexa flour 488 goat anti-rabbit (Invitrogen, Eugene, OR, USA #A11034) and Alexa flour 555 goat anti-rat (Invitrogen, Eugene, OR, USA #A11034) secondary antibodies diluted 1:500 in 0.25% Tween-20. Images were captured on a Zeiss 510 Meta confocal microscope, 63x/1.4 oil. Orthogonal views were constructed in FIJI imaging software.

Time lapse microscopy (TLM)

Primary bone marrow-derived macrophages (BMDM) were prepared from C57BL/6 mice (7–9 weeks old) [105]. Briefly, bone marrow collected from mouse femurs were mechanically homogenized and treated with red blood lysis buffer (8.29 g/l NH_4Cl, 1 g/l $KHCO_3$, 0.0372 g/l EDTA, pH = 7.4) before resuspending the washed bone marrow in differentiation medium (complete RPMI medium (R10) supplemented with 20% L929 conditioned media (LCM)). After 3 days, the cultures received an additional dose of 20% LCM. Between 16–24 hours prior to co-culture with fungal cells, the differentiated BMDM (~80–90% confluence) were collected by scraping, suspended in R10 medium, counted, and seeded at 1 x 10^6 cells/dish in a 35-mm imaging dish (ibidi, Martinsried, Germany). Wildtype SCADH1G4A (*ADH1/*P_{ADH1}*-GFP*) and CFG240 (*put1-/- ADH1/*P_{ADH1}*-RFP*) *C. albicans* cells from overnight YPD liquid cultures were collected by centrifugation, washed 3X with sterile PBS, and diluted to $OD_{600} \approx 0.5$ in HBSS. Fungal cells were mixed 1:1 (v/v) in a sterile Eppendorf tube and vortexed. The BMDM cells were pre-washed 2 times with HBSS and an aliquot of mixed fungal cells in HBSS was added at a MOI of 3:1 (C:M). The co-cultures were incubated for approximately 30 min in the humidified chamber, after which they were washed 5X with HBSS and 1X with CO_2-independent medium to remove non-phagocytosed fungal cells. CO_2-independent medium was added to the dish and TLM was carried out using Zeiss Cell Observer system (63x/1.4 oil) equipped with appropriate filters to detect GFP and RFP. Images were acquired every 2 min for 5 h and then saved as movie at 10 fps.

Supporting information

S1 Fig. Hyphae-specific gene (*HSG*) expression in *C. albicans* grown in the presence of inducing amino acids.
(TIF)

S2 Fig. NanoLuc luciferase assay for analysis of Stp2 target gene expression. A. The *CAN1* promoter (P_{CAN1}) is responsive to extracellular amino acids. **B**. P_{CAN1}*-NanoLucPEST* expression is strictly dependent on a functional SPS sensor.
(TIF)

S3 Fig. Phenotypic characterization of CRISPR/Cas9-mediated gene inactivation in *C. albicans*. Verification of *ssy1*-/- strains. **B**. Verification of *csh3*-/- strains. **C**. Verification of *ira2*-/- strains. **D**. Verification of *car1*-/- strains. **E**. Verification of *dur1,2*-/- strains. **F**. Verification of *put1*-/-, *put2*-/- and *put3*-/- strains. **G**. Verification of the *put1*-/- *dur1,2*-/- double mutant strain.
(TIF)

S4 Fig. Growth curves of arginine catabolic-pathway mutants in different nitrogen sources.
(TIF)

S5 Fig. Mutants lacking *DUR1,2* retain the ability to alkalinize the growth medium when using arginine as sole carbon and nitrogen source.
(TIF)

S6 Fig. Mitochondrial oxygen consumption is carbon source dependent. A. Oxygen consumption of *C. albicans* wildtype cells (PMRCA18) grown in synthetic proline medium containing 2% glucose (SPD), 0.2% glucose ($SPD_{0.2\%}$) or 1% glycerol (SPG). **B**. Inhibitors of mitochondrial oxidative phosphorylation used to control assessment of oxygen consumption.
(TIF)

S7 Fig. Ras1/cAMP/PKA pathway signaling and Efg1-dependent transcription are required for amino acid-induced morphogenesis. A. Alanine, Glutamine or Serine induce hyphal growth in a Ras1- and Efg1-dependent manner. **B**. Hyperactive Ras1 ($RAS1^{G13V}$) bypasses methylene blue inhibition of hyphal growth.
(TIF)

S1 Text. Table—Strains used in this study.
(DOCX)

S2 Text. Table—Primers used in this study.
(DOCX)

S3 Text. Supporting figures—Legends.
(DOCX)

S4 Text. Supporting references.
(DOCX)

Acknowledgments

The authors would like to thank the members of Claes Andréasson, Martin Ott, and Per Ljungdahl laboratories (SU), and members of the Marie Curie-ITN ImResFun program for constructive comments throughout the course of this work. Gratitude is extended to Valmik Vyas and Gerard Fink (MIT, Cambridge, MA, USA) for providing the CRISPR/Cas9 cassettes and for the valuable suggestions. Patrick van Dijck (KUL, Leuven, Belgium), Karl Kuchler (MUV, Vienna, Austria), Joachim Morschhäuser (UW, Würzburg, Germany), Kenneth Nickerson and Ruvini Pathirana (UNL, Lincoln, NE, USA) are gratefully acknowledged for supplying strains and discussions; and Nora Grahl and Deborah Hogan (Dartmouth Medical School, Hanover, NH, USA) for helpful discussions. We also thank Stina Höglund, the Imaging Facility-Stockholm University, for assistance in microscopy.

Author Contributions

Conceptualization: Fitz Gerald S. Silao, Meliza Ward, Per O. Ljungdahl.

Data curation: Fitz Gerald S. Silao, Meliza Ward, Kicki Ryman, Axel Wallström, Björn Brindefalk, Klas Udekwu, Per O. Ljungdahl.

Formal analysis: Fitz Gerald S. Silao, Björn Brindefalk, Klas Udekwu, Per O. Ljungdahl.

Funding acquisition: Per O. Ljungdahl.

Investigation: Fitz Gerald S. Silao, Meliza Ward, Kicki Ryman, Axel Wallström, Björn Brindefalk, Klas Udekwu.

Methodology: Fitz Gerald S. Silao, Meliza Ward, Björn Brindefalk, Klas Udekwu.

Project administration: Per O. Ljungdahl.

Resources: Per O. Ljungdahl.

Software: Björn Brindefalk, Klas Udekwu.

Supervision: Klas Udekwu, Per O. Ljungdahl.

Validation: Axel Wallström.

Visualization: Fitz Gerald S. Silao, Meliza Ward, Kicki Ryman.

Writing – original draft: Fitz Gerald S. Silao, Per O. Ljungdahl.

Writing – review & editing: Fitz Gerald S. Silao, Meliza Ward, Björn Brindefalk, Klas Udekwu, Per O. Ljungdahl.

References

1. Moyes DL, Naglik JR. Mucosal immunity and *Candida albicans* infection. Clin Dev Immunol. 2011; 2011:346307. https://doi.org/10.1155/2011/346307 PMID: 21776285.
2. Kullberg BJ, Arendrup MC. Invasive Candidiasis. N Engl J Med. 2015; 373(15):1445–56. https://doi.org/10.1056/NEJMra1315399 PMID: 26444731.
3. Brown AJ, Brown GD, Netea MG, Gow NA. Metabolism impacts upon Candida immunogenicity and pathogenicity at multiple levels. Trends Microbiol. 2014; 22(11):614–22. https://doi.org/10.1016/j.tim.2014.07.001 PMID: 25088819.
4. Sudbery PE. Growth of *Candida albicans* hyphae. Nat Rev Microbiol. 2011; 9(10):737–48. https://doi.org/10.1038/nrmicro2636 PMID: 21844880.
5. Berman J. Morphogenesis and cell cycle progression in *Candida albicans*. Curr Opin Microbiol. 2006; 9(6):595–601. https://doi.org/10.1016/j.mib.2006.10.007 PMID: 17055773.
6. Sudbery P, Gow N, Berman J. The distinct morphogenic states of *Candida albicans*. Trends Microbiol. 2004; 12(7):317–24. https://doi.org/10.1016/j.tim.2004.05.008 PMID: 15223059.
7. Noble SM, Gianetti BA, Witchley JN. *Candida albicans* cell-type switching and functional plasticity in the mammalian host. Nat Rev Microbiol. 2016. https://doi.org/10.1038/nrmicro.2016.157 PMID: 27867199.
8. Lo HJ, Kohler JR, DiDomenico B, Loebenberg D, Cacciapuoti A, Fink GR. Nonfilamentous *C. albicans* mutants are avirulent. Cell. 1997; 90(5):939–49. PMID: 9298905.
9. Lorenz MC, Bender JA, Fink GR. Transcriptional response of *Candida albicans* upon internalization by macrophages. Eukaryot Cell. 2004; 3(5):1076–87. https://doi.org/10.1128/EC.3.5.1076-1087.2004 PMID: 15470236.
10. Braun BR, J AD. *TUP1*, *CPH1* and *EFG1* make independent contributions to filamentation in *Candida albicans*. Genetics. 2000; 155:56–67.
11. Land GA, McDonald WC, Stjernholm RL, Friedman L. Factors affecting filamentation in *Candida albicans*: changes in respiratory activity of *Candida albicans* during filamentation. Infect Immun. 1975; 12 (1):119–27. PMID: 1095490.
12. Land GA, McDonald WC, Stjernholm RL, Friedman TL. Factors affecting filamentation in *Candida albicans*: relationship of the uptake and distribution of proline to morphogenesis. Infect Immun. 1975; 11 (5):1014–23. PMID: 1091557.
13. Dabrowa N, Taxer SS, Howard DH. Germination of *Candida albicans* induced by proline. Infect Immun. 1976; 13(3):830–5. PMID: 5375.
14. Grahl N, Demers EG, Lindsay AK, Harty CE, Willger SD, Piispanen AE, et al. Mitochondrial Activity and Cyr1 Are Key Regulators of Ras1 Activation of *C. albicans* Virulence Pathways. PLoS Pathog. 2015; 11(8):e1005133. https://doi.org/10.1371/journal.ppat.1005133 PMID: 26317337.
15. Morales DK, Grahl N, Okegbe C, Dietrich LE, Jacobs NJ, Hogan DA. Control of *Candida albicans* metabolism and biofilm formation by *Pseudomonas aeruginosa* phenazines. MBio. 2013; 4(1): e00526–12. https://doi.org/10.1128/mBio.00526-12 PMID: 23362320.

16. Bambach A, Fernandes MP, Ghosh A, Kruppa M, Alex D, Li D, et al. Goa1p of *Candida albicans* localizes to the mitochondria during stress and is required for mitochondrial function and virulence. Eukaryot Cell. 2009; 8(11):1706–20. Epub 2009/09/01. https://doi.org/10.1128/EC.00066-09 PMID: 19717740.

17. Watanabe T, Ogasawara A, Mikami T, Matsumoto T. Hyphal formation of *Candida albicans* is controlled by electron transfer system. Biochem Biophys Res Commun. 2006; 348(1):206–11. https://doi.org/10.1016/j.bbrc.2006.07.066 PMID: 16876761.

18. McDonough JA, Bhattacherjee V, Sadlon T, Hostetter MK. Involvement of *Candida albicans* NADH dehydrogenase complex I in filamentation. Fungal Genet Biol. 2002; 36(2):117–27. Epub 2002/06/26. https://doi.org/10.1016/S1087-1845(02)00007-5 PMID: 12081465.

19. Monge RA, Roman E, Nombela C, Pla J. The MAP kinase signal transduction network in *Candida albicans*. Microbiology. 2006; 152(Pt 4):905–12. https://doi.org/10.1099/mic.0.28616-0 PMID: 16549655.

20. Stoldt VR, Sonneborn A, Leuker CE, Ernst JF. Efg1p, an essential regulator of morphogenesis of the human pathogen *Candida albicans*, is a member of a conserved class of bHLH proteins regulating morphogenetic processes in fungi. EMBO J. 1997; 16(8):1982–91. https://doi.org/10.1093/emboj/16.8.1982 PMID: 9155024.

21. Biswas S, Van Dijck P, Datta A. Environmental sensing and signal transduction pathways regulating morphopathogenic determinants of *Candida albicans*. Microbiol Mol Biol Rev. 2007; 71(2):348–76. https://doi.org/10.1128/MMBR.00009-06 PMID: 17554048.

22. Hogan DA, Sundstrom P. The Ras/cAMP/PKA signaling pathway and virulence in *Candida albicans*. Future Microbiol. 2009; 4(10):1263–70. https://doi.org/10.2217/fmb.09.106 PMID: 19995187.

23. Leberer E, Harcus D, Dignard D, Johnson L, Ushinsky S, Thomas DY, et al. Ras links cellular morphogenesis to virulence by regulation of the MAP kinase and cAMP signalling pathways in the pathogenic fungus *Candida albicans*. Mol Microbiol. 2001; 42(3):673–87. PMID: 11722734.

24. Feng Q, Summers E, Guo B, Fink G. Ras signaling is required for serum-induced hyphal differentiation in *Candida albicans*. J Bacteriol. 1999; 181(20):6339–46. PMID: 10515923.

25. Inglis DO, Sherlock G. Ras signaling gets fine-tuned: regulation of multiple pathogenic traits of *Candida albicans*. Eukaryot Cell. 2013; 12(10):1316–25. https://doi.org/10.1128/EC.00094-13 PMID: 23913542.

26. Fang HM, Wang Y. RA domain-mediated interaction of Cdc35 with Ras1 is essential for increasing cellular cAMP level for *Candida albicans* hyphal development. Mol Microbiol. 2006; 61(2):484–96. https://doi.org/10.1111/j.1365-2958.2006.05248.x PMID: 16856944.

27. Zou H, Fang HM, Zhu Y, Wang Y. *Candida albicans* Cyr1, Cap1 and G-actin form a sensor/effector apparatus for activating cAMP synthesis in hyphal growth. Mol Microbiol. 2010; 75(3):579–91. https://doi.org/10.1111/j.1365-2958.2009.06980.x PMID: 19943905.

28. Rocha CR, Schroppel K, Harcus D, Marcil A, Dignard D, Taylor BN, et al. Signaling through adenylyl cyclase is essential for hyphal growth and virulence in the pathogenic fungus *Candida albicans*. Mol Biol Cell. 2001; 12(11):3631–43. https://doi.org/10.1091/mbc.12.11.3631 PMID: 11694594.

29. Hogan DA, Muhlschlegel FA. *Candida albicans* developmental regulation: adenylyl cyclase as a coincidence detector of parallel signals. Curr Opin Microbiol. 2011; 14(6):682–6. https://doi.org/10.1016/j.mib.2011.09.014 PMID: 22014725.

30. Wang Y. Fungal adenylyl cyclase acts as a signal sensor and integrator and plays a central role in interaction with bacteria. PLoS Pathog. 2013; 9(10):e1003612. https://doi.org/10.1371/journal.ppat.1003612 PMID: 24130478.

31. Klengel T, Liang WJ, Chaloupka J, Ruoff C, Schroppel K, Naglik JR, et al. Fungal adenylyl cyclase integrates CO_2 sensing with cAMP signaling and virulence. Curr Biol. 2005; 15(22):2021–6. https://doi.org/10.1016/j.cub.2005.10.040 PMID: 16303561.

32. Ghosh S, Navarathna DH, Roberts DD, Cooper JT, Atkin AL, Petro TM, et al. Arginine-induced germ tube formation in *Candida albicans* is essential for escape from murine macrophage line RAW 264.7. Infect Immun. 2009; 77(4):1596–605. https://doi.org/10.1128/IAI.01452-08 PMID: 19188358.

33. Maidan MM, Thevelein JM, Van Dijck P. Carbon source induced yeast-to-hypha transition in *Candida albicans* is dependent on the presence of amino acids and on the G-protein-coupled receptor Gpr1. Biochem Soc Trans. 2005; 33(Pt 1):291–3. https://doi.org/10.1042/BST0330291 PMID: 15667329.

34. Miwa T, Takagi Y, Shinozaki M, Yun CW, Schell WA, Perfect JR, et al. Gpr1, a putative G-protein-coupled receptor, regulates morphogenesis and hypha formation in the pathogenic fungus *Candida albicans*. Eukaryot Cell. 2004; 3(4):919–31. https://doi.org/10.1128/EC.3.4.919-931.2004 PMID: 15302825.

35. Ballou ER, Avelar GM, Childers DS, Mackie J, Bain JM, Wagener J, et al. Lactate signalling regulates fungal beta-glucan masking and immune evasion. Nat Microbiol. 2016; 2:16238. https://doi.org/10.1038/nmicrobiol.2016.238 PMID: 27941860.

36. Martínez P, Ljungdahl PO. Divergence of Stp1 and Stp2 transcription factors in *Candida albicans* places virulence factors required for proper nutrient acquisition under amino acid control. Mol Cell Biol. 2005; 25(21):9435–46. https://doi.org/10.1128/MCB.25.21.9435-9446.2005 PMID: 16227594.

37. Martínez P, Ljungdahl PO. An ER packaging chaperone determines the amino acid uptake capacity and virulence of *Candida albicans*. Mol Microbiol. 2004; 51(2):371–84. https://doi.org/10.1046/j.1365-2958.2003.03845.x PMID: 14756779.

38. Brega E, Zufferey R, Mamoun CB. *Candida albicans* Csy1p is a nutrient sensor important for activation of amino acid uptake and hyphal morphogenesis. Eukaryot Cell. 2004; 3(1):135–43. https://doi.org/10.1128/EC.3.1.135-143.2004 PMID: 14871944.

39. Dabas N, Morschhäuser J. A transcription factor regulatory cascade controls secreted aspartic protease expression in *Candida albicans*. Mol Microbiol. 2008; 69(3):586–602. https://doi.org/10.1111/j.1365-2958.2008.06297.x PMID: 18547391.

40. Felk A, Kretschmar M, Albrecht A, Schaller M, Beinhauer S, Nichterlein T, et al. *Candida albicans* hyphal formation and the expression of the Efg1-regulated proteinases Sap4 to Sap6 are required for the invasion of parenchymal organs. Infect Immun. 2002; 70(7):3689–700. https://doi.org/10.1128/IAI.70.7.3689-3700.2002 PMID: 12065511.

41. Hall MP, Unch J, Binkowski BF, Valley MP, Butler BL, Wood MG, et al. Engineered luciferase reporter from a deep sea shrimp utilizing a novel imidazopyrazinone substrate. ACS Chem Biol. 2012; 7(11):1848–57. https://doi.org/10.1021/cb3002478 PMID: 22894855.

42. Liu H, Kohler J, Fink GR. Suppression of hyphal formation in *Candida albicans* by mutation of a *STE12* homolog. Science. 1994; 266(5191):1723–6. PMID: 7992058.

43. Custot J, Moali C, Brollo M, Boucher JL, Delaforge M, Mansuy D, et al. A new α-amino acid N-w-hydroxy-nor-L-arginine: A highly-affinity inhibitor of arginase well adapted to bind to its manganese cluster. J Am Chem Soc. 1997; 119(17):4086–7. https://doi.org/10.1021/ja970285o

44. Zhang M, White TA, Schuermann JP, Baban BA, Becker DF, Tanner JJ. Structures of the *Escherichia coli* PutA proline dehydrogenase domain in complex with competitive inhibitors. Biochemistry. 2004; 43(39):12539–48. Epub 2004/09/29. https://doi.org/10.1021/bi048737e PMID: 15449943.

45. Zhu W, Gincherman Y, Docherty P, Spilling CD, Becker DF. Effects of proline analog binding on the spectroscopic and redox properties of PutA. Arch Biochem Biophys. 2002; 408(1):131–6. Epub 2002/12/18. PMID: 12485611.

46. Visarius TM, Stucki JW, Lauterburg BH. Stimulation of respiration by methylene blue in rat liver mitochondria. FEBS Lett. 1997; 412(1):157–60. Epub 1997/07/21. PMID: 9257711.

47. Lee KK, Boelsterli UA. Bypassing the compromised mitochondrial electron transport with methylene blue alleviates efavirenz/isoniazid-induced oxidant stress and mitochondria-mediated cell death in mouse hepatocytes. Redox Biol. 2014; 2:599–609. Epub 2014/12/03. https://doi.org/10.1016/j.redox.2014.03.003 PMID: 25460728.

48. Rich PR, Mischis LA, Purton S, Wiskich JT. The sites of interaction of triphenyltetrazolium chloride with mitochondrial respiratory chains. FEMS Microbiol Lett. 2001; 202(2):181–7. Epub 2001/08/25. https://doi.org/10.1111/j.1574-6968.2001.tb10801.x PMID: 11520612.

49. Candeias LP, MacFarlane DPS, M S.L.W., Maidwell NL, Roeschlaub CA, Sammes PG, et al. The catalysed NADH reduction of resazurin to resorufin. J Chem Soc. 1998;(11):2333–4. https://doi.org/10.1039/A806431H

50. Marczak JE, Brandriss MC. Isolation of constitutive mutations affecting the proline utilization pathway in *Saccharomyces cerevisiae* and molecular analysis of the *PUT3* transcriptional activator. Mol Cell Biol. 1989; 9(11):4696–705. Epub 1989/11/01. PMID: 2689861.

51. Siddiqui AH, Brandriss MC. The *Saccharomyces cerevisiae PUT3* activator protein associates with proline-specific upstream activation sequences. Mol Cell Biol. 1989; 9(11):4706–12. Epub 1989/11/01. PMID: 2689862.

52. Tebung WA, Omran RP, Fulton DL, Morschhäuser J, Whiteway M. Put3 positively regulates proline utilization in *Candida albicans*. mSphere. 2017; 2(6). Epub 2017/12/16. https://doi.org/10.1128/mSphere.00354-17 PMID: 29242833.

53. Vylkova S, Carman AJ, Danhof HA, Collette JR, Zhou H, Lorenz MC. The fungal pathogen *Candida albicans* autoinduces hyphal morphogenesis by raising extracellular pH. MBio. 2011; 2(3):e00055–11. https://doi.org/10.1128/mBio.00055-11 PMID: 21586647.

54. Vemuri GN, Eiteman MA, McEwen JE, Olsson L, Nielsen J. Increasing NADH oxidation reduces overflow metabolism in *Saccharomyces cerevisiae*. Proc Natl Acad Sci U S A. 2007; 104(7):2402–7. https://doi.org/10.1073/pnas.0607469104 PMID: 17287356.

55. Kayikci O, Nielsen J. Glucose repression in *Saccharomyces cerevisiae*. FEMS Yeast Res. 2015; 15 (6). Epub 2015/07/25. https://doi.org/10.1093/femsyr/fov068 PMID: 26205245.

56. Ljungdahl PO, Daignan-Fornier B. Regulation of amino acid, nucleotide, and phosphate metabolism in *Saccharomyces cerevisiae*. Genetics. 2012; 190(3):885–929. https://doi.org/10.1534/genetics.111.133306 PMID: 22419079.

57. Liao WL, Ramon AM, Fonzi WA. *GLN3* encodes a global regulator of nitrogen metabolism and virulence of *C. albicans*. Fungal Genet Biol. 2008; 45(4):514–26. https://doi.org/10.1016/j.fgb.2007.08.006 PMID: 17950010.

58. Skrzypek MS, Binkley J, Binkley G, Miyasato SR, Simison M, Sherlock G. The Candida Genome Database (CGD): incorporation of Assembly 22, systematic identifiers and visualization of high throughput sequencing data. Nucleic Acids Res. 2017; 45(D1):D592–D6. Epub 2016/10/16. https://doi.org/10.1093/nar/gkw924 PMID: 27738138.

59. Holmes AR, Shepherd MG. Proline-induced germ-tube formation in *Candida albicans*: role of proline uptake and nitrogen metabolism. J Gen Microbiol. 1987; 133(11):3219–28. https://doi.org/10.1099/00221287-133-11-3219 PMID: 3328774.

60. Brandriss MC, Magasanik B. Genetics and physiology of proline utilization in *Saccharomyces cerevisiae*: enzyme induction by proline. J Bacteriol. 1979; 140(2):498–503. PMID: 387737.

61. Brandriss MC, Magasanik B. Proline: an essential intermediate in arginine degradation in *Saccharomyces cerevisiae*. J Bacteriol. 1980; 143(3):1403–10. PMID: 6997271.

62. Brandriss MC, Magasanik B. Subcellular compartmentation in control of converging pathways for proline and arginine metabolism in *Saccharomyces cerevisiae*. J Bacteriol. 1981; 145(3):1359–64. PMID: 7009582.

63. Steegborn C. Structure, mechanism, and regulation of soluble adenylyl cyclases—similarities and differences to transmembrane adenylyl cyclases. Biochim Biophys Acta. 2014; 1842(12 Pt B):2535–47. Epub 2014/09/07. https://doi.org/10.1016/j.bbadis.2014.08.012 PMID: 25193033.

64. Xue Y, Batlle M, Hirsch JP. *GPR1* encodes a putative G protein-coupled receptor that associates with the Gpa2p Galpha subunit and functions in a Ras-independent pathway. EMBO J. 1998; 17(7):1996–2007. https://doi.org/10.1093/emboj/17.7.1996 PMID: 9524122.

65. Maidan MM, De Rop L, Serneels J, Exler S, Rupp S, Tournu H, et al. The G protein-coupled receptor Gpr1 and the Galpha protein Gpa2 act through the cAMP-protein kinase A pathway to induce morphogenesis in *Candida albicans*. Mol Biol Cell. 2005; 16(4):1971–86. https://doi.org/10.1091/mbc.E04-09-0780 PMID: 15673611.

66. Bicho CC, de Lima Alves F, Chen ZA, Rappsilber J, Sawin KE. A genetic engineering solution to the "arginine conversion problem" in stable isotope labeling by amino acids in cell culture (SILAC). Mol Cell Proteomics. 2010; 9(7):1567–77. https://doi.org/10.1074/mcp.M110.000208 PMID: 20460254.

67. Park SK, Liao L, Kim JY, Yates JR 3rd. A computational approach to correct arginine-to-proline conversion in quantitative proteomics. Nat Methods. 2009; 6(3):184–5. Epub 2009/02/28. https://doi.org/10.1038/nmeth0309-184 PMID: 19247291.

68. Lossner C, Warnken U, Pscherer A, Schnolzer M. Preventing arginine-to-proline conversion in a cell-line-independent manner during cell cultivation under stable isotope labeling by amino acids in cell culture (SILAC) conditions. Anal Biochem. 2011; 412(1):123–5. Epub 2011/01/19. https://doi.org/10.1016/j.ab.2011.01.011 PMID: 21241653.

69. Van Hoof D, Pinkse MW, Oostwaard DW, Mummery CL, Heck AJ, Krijgsveld J. An experimental correction for arginine-to-proline conversion artifacts in SILAC-based quantitative proteomics. Nat Methods. 2007; 4(9):677–8. Epub 2007/09/01. https://doi.org/10.1038/nmeth0907-677 PMID: 17762871.

70. Nickerson WJ, and Edwards G.A. Studies on the physiological bases of morphogenesis in fungi. I. The respiratory metabolism of dimorphic pathogenic fungi. J Gen Physiol. 1949; 33(1):41–55. PMID: 18139007

71. Gancedo JM. Yeast carbon catabolite repression. Microbiol Mol Biol Rev. 1998; 62(2):334–61. Epub 1998/06/10. PMID: 9618445.

72. Pronk JT, Yde Steensma H, Van Dijken JP. Pyruvate metabolism in *Saccharomyces cerevisiae*. Yeast. 1996; 12(16):1607–33. Epub 1996/12/01. https://doi.org/10.1002/(SICI)1097-0061(199612)12:16%3C1607::AID-YEA70%3E3.0.CO;2-4 PMID: 9123965.

73. Niimi M, Kamiyama A, Tokunaga M. Respiration of medically important *Candida* species and *Saccharomyces cerevisiae* in relation to glucose effect. J Med Vet Mycol. 1988; 26(3):195–8. Epub 1988/06/01. PMID: 3050010.

74. Sabina J, Brown V. Glucose sensing network in *Candida albicans*: a sweet spot for fungal morphogenesis. Eukaryot Cell. 2009; 8(9):1314–20. https://doi.org/10.1128/EC.00138-09 PMID: 19617394.

75. Askew C, Sellam A, Epp E, Hogues H, Mullick A, Nantel A, et al. Transcriptional regulation of carbohydrate metabolism in the human pathogen *Candida albicans*. PLoS Pathog. 2009; 5(10):e1000612. Epub 2009/10/10. https://doi.org/10.1371/journal.ppat.1000612 PMID: 19816560.

76. Johnston M. Feasting, fasting and fermenting. Glucose sensing in yeast and other cells. Trends Genet. 1999; 15(1):29–33. Epub 1999/03/24. PMID: 10087931.

77. Kraidlova L, Schrevens S, Tournu H, Van Zeebroeck G, Sychrova H, Van Dijck P. Characterization of the *Candida albicans* amino acid permease family: Gap2 is the only general amino acid permease and Gap4 is an S-adenosylmethionine (SAM) transporter required for SAM-induced morphogenesis. mSphere. 2016; 1(6). Epub 2016/12/29. https://doi.org/10.1128/mSphere.00284-16 PMID: 28028545.

78. Dabrowa N, Howard DH. Proline uptake in *Candida albicans*. J Gen Microbiol. 1981; 127(2):391–7. https://doi.org/10.1099/00221287-127-2-391 PMID: 7045279.

79. Jimenez-Lopez C, Collette JR, Brothers KM, Shepardson KM, Cramer RA, Wheeler RT, et al. *Candida albicans* induces arginine biosynthetic genes in response to host-derived reactive oxygen species. Eukaryot Cell. 2013; 12(1):91–100. https://doi.org/10.1128/EC.00290-12 PMID: 23143683.

80. Kitamoto K, Yoshizawa K, Ohsumi Y, Anraku Y. Dynamic aspects of vacuolar and cytosolic amino acid pools of *Saccharomyces cerevisiae*. J Bacteriol. 1988; 170(6):2683–6. PMID: 3131304.

81. Martins RM, Covarrubias C, Rojas RG, Silber AM, Yoshida N. Use of L-proline and ATP production by *Trypanosoma cruzi* metacyclic forms as requirements for host cell invasion. Infect Immun. 2009; 77 (7):3023–32. Epub 2009/05/13. https://doi.org/10.1128/IAI.00138-09 PMID: 19433547.

82. Mantilla BS, Marchese L, Casas-Sanchez A, Dyer NA, Ejeh N, Biran M, et al. Proline metabolism is essential for *Trypanosoma brucei brucei* survival in the Tsetse vector. PLoS Pathog. 2017; 13(1): e1006158. Epub 2017/01/24. https://doi.org/10.1371/journal.ppat.1006158 PMID: 28114403.

83. Tonelli RR, Silber AM, Almeida-de-Faria M, Hirata IY, Colli W, Alves MJ. L-proline is essential for the intracellular differentiation of *Trypanosoma cruzi*. Cell Microbiol. 2004; 6(8):733–41. Epub 2004/07/09. https://doi.org/10.1111/j.1462-5822.2004.00397.x PMID: 15236640.

84. Ebikeme CE, Peacock L, Coustou V, Riviere L, Bringaud F, Gibson WC, et al. N-acetyl D-glucosamine stimulates growth in procyclic forms of *Trypanosoma brucei* by inducing a metabolic shift. Parasitology. 2008; 135(5):585–94. https://doi.org/10.1017/S0031182008004241 PMID: 18371239.

85. Vylkova S, Lorenz MC. Modulation of phagosomal pH by *Candida albicans* promotes hyphal morphogenesis and requires Stp2p, a regulator of amino acid transport. PLoS Pathog. 2014; 10(3):e1003995. https://doi.org/10.1371/journal.ppat.1003995 PMID: 24626429.

86. Velasco I, Tenreiro S, Calderon IL, André B. *Saccharomyces cerevisiae* Aqr1 is an internal-membrane transporter involved in excretion of amino acids. Eukaryotic Cell. 2004; 3(6):1492–503. https://doi.org/10.1128/EC.3.6.1492-1503.2004 PMID: 15590823

87. Hess DC, Lu W, Rabinowitz JD, Botstein D. Ammonium toxicity and potassium limitation in yeast. PLoS Biol. 2006; 4(11):e351. Epub 2006/10/20. https://doi.org/10.1371/journal.pbio.0040351 PMID: 17048990.

88. Fleck CB, Schöbel F, Brock M. Nutrient acquisition by pathogenic fungi: Nutrient availability, pathway regulation, and differences in substrate utilization. International Journal of Medical Microbiology. 2011; 301(5):400–7. https://doi.org/10.1016/j.ijmm.2011.04.007 PMID: 21550848

89. Olive AJ, Sassetti CM. Metabolic crosstalk between host and pathogen: sensing, adapting and competing. Nat Rev Microbiol. 2016; 14(4):221–34. https://doi.org/10.1038/nrmicro.2016.12 PMID: 26949049.

90. Yuan X, Mitchell BM, Wilhelmus KR. Expression of matrix metalloproteinases during experimental *Candida albicans* keratitis. Invest Ophthalmol Vis Sci. 2009; 50(2):737–42. https://doi.org/10.1167/iovs.08-2390 PMID: 19171647.

91. Vyas VK, Barrasa MI, Fink GR. A *Candida albicans* CRISPR system permits genetic engineering of essential genes and gene families. Sci Adv. 2015; 1(3):1–6. http://dx.doi.org/10.1126/sciadv.1500248.

92. Vyas VK, Bushkin GG, Bernstein DA, Getz MA, Sewastianik M, Barrasa MI, et al. New CRISPR mutagenesis strategies reveal variation in repair mechanisms among fungi. mSphere. 2018; 3(2). Epub 2018/04/27. https://doi.org/10.1128/mSphere.00154-18 PMID: 29695624.

93. Farboud B, M BJ. Dramatic enhancement of genome editing by CRISPR:Cas9 through improved guide RNA design. Genetics. 2015; 199:959–71. https://doi.org/10.1534/genetics.115.175166 PMID: 25695951

94. Reuss O, Vik A, Kolter R, Morschhäuser J. The *SAT1* flipper, an optimized tool for gene disruption in *Candida albicans*. Gene. 2004; 341:119–27. https://doi.org/10.1016/j.gene.2004.06.021 PMID: 15474295.

95. Davis MM, Alvarez FJ, Ryman K, Holm AA, Ljungdahl PO, Engström Y. Wild-type *Drosophila melanogaster* as a model host to analyze nitrogen source dependent virulence of *Candida albicans*. PLoS One. 2011; 6(11):e27434. https://doi.org/10.1371/journal.pone.0027434 PMID: 22110651.

96. Nurk S, Bankevich A, Antipov D, Gurevich AA, Korobeynikov A, Lapidus A, et al. Assembling single-cell genomes and mini-metagenomes from chimeric MDA products. J Comput Biol. 2013; 20(10):714–37. Epub 2013/10/08. https://doi.org/10.1089/cmb.2013.0084 PMID: 24093227.

97. Kolmogorov M, Raney B, Paten B, Pham S. Ragout-a reference-assisted assembly tool for bacterial genomes. Bioinformatics. 2014; 30(12):i302–9. Epub 2014/06/17. https://doi.org/10.1093/bioinformatics/btu280 PMID: 24931998.

98. Minkin I, Pham H, Starostina E, Vyahhi N, Pham S. C-Sibelia: an easy-to-use and highly accurate tool for bacterial genome comparison. F1000Res. 2013; 2:258. Epub 2013/01/01. https://doi.org/10.12688/f1000research.2-258.v1 PMID: 25110578.

99. Gurevich A, Saveliev V, Vyahhi N, Tesler G. QUAST: quality assessment tool for genome assemblies. Bioinformatics. 2013; 29(8):1072–5. Epub 2013/02/21. https://doi.org/10.1093/bioinformatics/btt086 PMID: 23422339.

100. Masser AE, Kandasamy G, Kaimal JM, Andréasson C. Luciferase NanoLuc as a reporter for gene expression and protein levels in *Saccharomyces cerevisiae*. Yeast. 2016; 33(5):191–200. Epub 2016/02/11. https://doi.org/10.1002/yea.3155 PMID: 26860732.

101. Hnisz D, Majer O, Frohner IE, Komnenovic V, Kuchler K. The Set3/Hos2 histone deacetylase complex attenuates cAMP/PKA signaling to regulate morphogenesis and virulence of *Candida albicans*. PLoS Pathog. 2010; 6(5):e1000889. Epub 2010/05/21. https://doi.org/10.1371/journal.ppat.1000889 PMID: 20485517.

102. Silve S, Volland C, Garnier C, Jund R, Chevallier MR, Haguenauer-Tsapis R. Membrane insertion of uracil permease, a polytopic yeast plasma membrane protein. Mol Cell Biol. 1991; 11(2):1114–24. PMID: 1846664.

103. Carillo P, Mastrolonardo G, Nacca F, Parisi D, Verlotta A, Fuggi A. Nitrogen metabolism in durum wheat under salinity: accumulation of proline and glycine betaine. Functional Plant Biology [Internet]. 2008; 35(5):[412–26 pp.]. Available from: http://dx.doi.org/10.1071/FP08108.

104. Cihlar RL, Calderone RA. *Candida albicans*: methods and protocols. Preface. Methods Mol Biol. 2009; 499:v. Epub 2009/03/04. PMID: 19253458.

105. Weischenfeldt J, Porse B. Bone Marrow-Derived Macrophages (BMM): Isolation and Applications. CSH Protoc. 2008; 2008:pdb prot5080. Epub 2008/01/01. https://doi.org/10.1101/pdb.prot5080 PMID: 21356739.